Title: Nanolattices - An Emerging Class of Mechanical Metamaterials

Jens Bauer*, Lucas R. Meza, Tobias A. Schaedler, Ruth Schwaiger, Xiaoyu Zheng, Lorenzo Valdevit

Dr. J. Bauer, Prof. L. Valdevit
Department of Mechanical and Aerospace Engineering, University of California Irvine,
CA 92697, USA
E-mail: jens.bauer@uci.edu

Dr. J. Bauer, Dr. R. Schwaiger
Institute for Applied Materials, Karlsruhe Institute of Technology,
Hermann-von-Helmholtz-Platz 1, Eggenstein-Leopoldshafen, 76344, Germany

Dr. L. R. Meza
Engineering Department, Trumpington Street, Cambridge, CB2 1PZ, UK

Dr. T. A. Schaedler
HRL Laboratories Limited Liability Company, Malibu, CA 90265, USA

Prof. X. Zheng
Department of Mechanical Engineering, Virginia Tech,
445 Goodwin Hall,635 Prices Fork Road - MC 0238, Blacksburg, VA 24061, USA

In 1903 Alexander Graham Bell developed a design principle to generate lightweight, mechanically robust lattice structures based on triangular cells; this has since found broad application in lightweight design. Over one hundred years later, the same principle is being used in the fabrication of nanolattice materials, namely lattice structures comprised of nanoscale constituents. Taking advantage of size-dependent properties typical of nanoparticles, nanowires, and thin films, nanolattices redefine the limits of the accessible material property space throughout different disciplines. We review the exceptional mechanical performance of nanolattices, including their ultra-high strength, damage tolerance, and stiffness, and examine their potential for multifunctional applications beyond mechanics. The efficient integration of architecture and size-affected properties is key to further develop nanolattices. The introduction of hierarchical architecture is an effective tool in enhancing mechanical properties, and the eventual goal of nanolattice design may be to replicate the intricate hierarchies and functionalities observed in biological materials. Additive manufacturing and self-assembly techniques enabled lattice design at the nanoscale, the scaling-up of nanolattice fabrication is currently the major challenge to their widespread use in technological applications.

1. Introduction

No solid material considerably lighter than water has been reported to date. To decrease density beyond this point, materials must have a porosity, which generally comes at the cost of a disproportional degradation of properties. For example, a foam with a relative density ($\bar{\rho}$), i.e. the volume fraction, of 10% will have a stiffness and strength that are 0.3% and 0.9% of the constitutive bulk material, respectively. In this sense, lighter than water and as strong as steel is intuitively a utopian property combination, yet it has recently been achieved with nanolattice materials.[1–3]

Material availability and advances in processing have defined human progress since the Stone Age, the modern frontier for material design is that of nanomaterials. One- and two-dimensional nanomaterials, such as nanowires and thin films, are known to have exceptional properties, which are intrinsically coupled to dimensional constraints such as surface-to-volume ratios. When nanowires and thin films are scaled up, their size-affected properties are lost. Similarly, when they are clustered in a composite, interfaces weaken their overall performance. To overcome this dilemma one could think of highly ordered three-dimensional architectures constructed from nanowires or thin films. This is what long remained technologically infeasible - this is what nanolattice materials are.

Nanolattices have been rapidly developed over the past few years, redefining the limits of the accessible material property space. The key driving force for this advance was the evolution of high-precision additive manufacturing techniques, such as self-propagating photopolymer waveguides (SPPW)[4], projection micro-stereolithography (PµSL)[5], and direct laser writing (DLW)[6,7], which have led to the production of progressively smaller lattice structures **(Figure 1)** reaching unit cell sizes below 1 µm.[8] Self-assembly techniques have been used to synthesize nanolattices with unit cell sizes down to the order of 50 nm.[2,3,9] Genetic engineering may be

another potential method for nanolattice fabrication.[10–12] Micro- and nanolattices possess unparalleled mechanical properties at extremely low densities, including effective strengths of up to 1 GPa[1–3,9,13,14], high deformability and recoverability with brittle constituent materials[13,15–18], and ultra-high stiffness[19], all despite being comprised of 50-99.9% air. Also, auxetic structures with negative Poisson's ratio[20], pentamode lattices with near zero shear modulus and a resulting fluid-like behavior[21], and exceptional non-mechanical properties, such as optical cloaking[22,23] and broadband electromagnetic polarization[24], have been demonstrated.
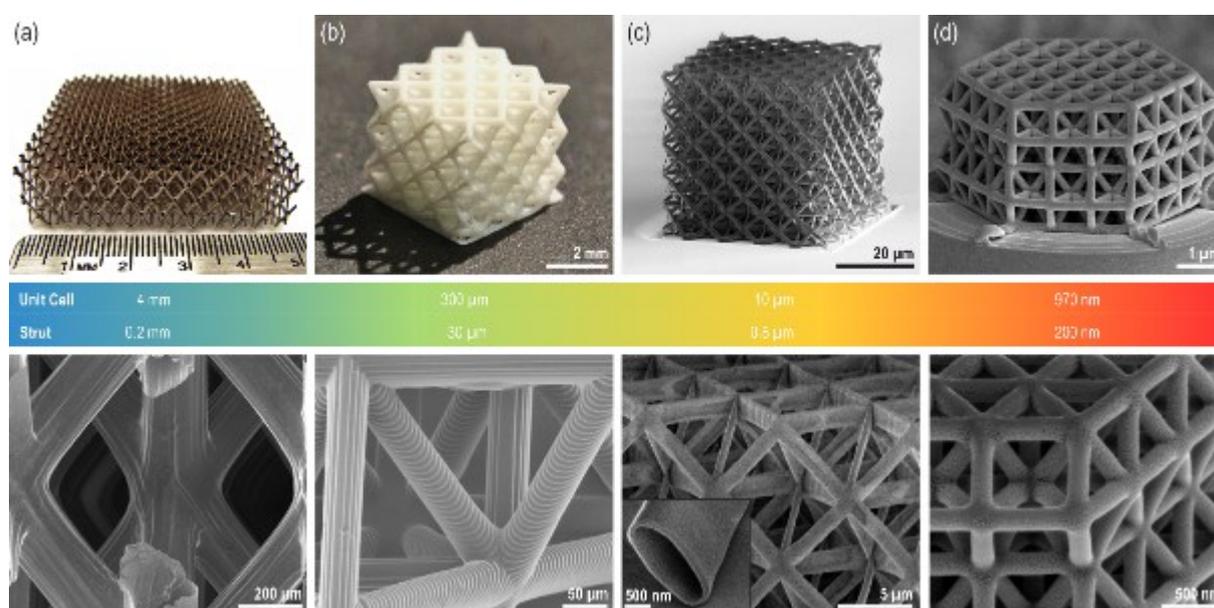

Figure 1. **Lattice miniaturization – from the millimeter- to the nanoscale.** Characteristic unit cell dimensions and diameters of individual struts are indicated. (a) Hollow-beam nickel lattice, manufactured using SPPW polymer templates, electroless nickel plating, and base etching to remove the polymer. (b) Solid-beam alumina lattice fabricated by PµSL with a nanoparticle loaded resist and subsequent sintering. (c) Hollow-beam alumina lattice fabricated by DLW, atomic layer deposition and oxygen plasma etching. (d) Solid-beam glassy carbon lattice made by DLW and subsequent pyrolysis. Adopted from [1] and reproduced with permission, [15] 2011, [19] 2014, [13] 2014, The American Association of the Advancement of Science.

While the concept of resilient lattice architecture is more than a century old and goes back to Alexander Graham Bell[25] and Buckminster Fuller[26], today lattices can for the first time be made small enough to actually exploit nanoscale properties. It is this unique feature, which facilitates extraordinary strength, sometimes higher than that of the corresponding fully dense

bulk material, as well as optical or electromagnetic properties. Other mechanical characteristics of nanolattices, including ductile-like behavior and high stiffness, arise from scale-independent structural effects.

At the nanoscale, *size effects* can tremendously alter the mechanical[27–31], magnetic[27], thermal[32,33], and electrical[34,35] properties of a material compared to its corresponding bulk behavior. This is related to microstructural constraints, such as the size and distribution of dislocations, grain boundaries, cracks and voids, which in small scales can be affected by dimensional constraints. The presence of defects can have various effects in different materials systems. For example, plastic flow in metals occurs via dislocation motion, and defects such as grain boundaries hinder this process; thus, the yield strength of polycrystalline metals generally increases as the grain size is reduced.[36] The chemical bonds in ceramics do not allow plastic deformation at room temperature, and stress concentrations at crack tips cannot be relieved by localized plastic flow; the size of cracks is therefore the limiting factor for their strength. The size of any defect is limited by the overall dimensions of an object, meaning the smaller the object, the higher its strength will be. Mechanisms governing strength can be more complex[27,30,31], but there is a clear overall trend that "smaller is stronger". Metallic and ceramic ultra-strong nanoscale materials have been reported, such as 40 nm thin and 5.6 GPa strong gold wires[37], 20 nm thin and 18 GPa strong silicon wires[38], and carbon nanotubes (CNTs) and graphene reaching stresses as high as 100–130 GPa[37]. Additionally, properties like ductility in silicon nanowires[38–40] and metallic glass nanopillars[41,42], increased Young's modulus in carbon[43–46] and nanoporous gold[47], as well as notch insensitivity in gold nanowires[48] have also been observed. Future nanolattices may be able to further capitalize on these enhanced nanomaterial properties.

Using classical material fabrication methods, there appears to be little room for further expansion of the accessible material property space. To develop new materials, three

fundamental approaches have been identified:[49] (I) By manipulation of the *chemistry*, metal alloys, polymer formulations, and ceramic or glass compositions may be developed. (II) Manipulating the *microstructure* by thermo-mechanical processing controls the distribution of defects and phases, thereby modifying a material's properties without changing the chemistry. Searching for lighter, stronger, stiffer, and more durable materials, both approaches have systematically been exploited over centuries with great success. (III) Controlling the *architecture* of multiple materials (composites) or a single material and space (cellular materials) creates hybrid materials. Introducing architecture into materials design allows for the tailoring of a vast range of material property combinations depending on the topology, i.e. the spatial layout of constituent materials.

The mechanical properties of cellular materials are defined by their constituent material properties, relative density and architecture, and they are traditionally classified as *bending-* or *stretching-dominated* depending on their topology.[50] Stochastic structures such as foams commonly deform by bending of their ligaments, resulting in an inhomogeneous stress distribution and therefore poor material utilization. The effective strength and stiffness of bending-dominated structures scales with their relative density as $\sigma_{eff} \propto \bar{\rho}^{1.5}$ and $E_{eff} \propto \bar{\rho}^2$ respectively.[51] An ideal stretching-dominated material deforms via uniaxial compression and tension of its members, and has a linear scaling with the relative density of both strength ($\sigma_{eff} \propto \bar{\rho}$) and stiffness ($E_{eff} \propto \bar{\rho}$).

Bending- or stretching-dominated behavior of an open-cell topology generally depends on the rigidity of its pin-jointed counterpart **(Figure 2)**.[52] In 2D, the triangle is the only rigid polygon, and in 3D, polyhedral cells with fully triangulated surfaces are rigid. The connectivity (Z) of a structure, namely the average number of elements connected at a node, is a good indicator of rigidity. A topology constructed from rigid unit cells is necessarily fully rigid and stretching-dominated, with $Z = 6$ and $Z = 12$ for the 2D and 3D cases, respectively (Figure 2a).

Topologies with lower connectivities can be periodically-rigid and theoretically still stretching-dominated (Figure 2b-c), but they are more sensitive to imperfections, which may easily activate deformation mechanisms that can cause bending. Non-rigid topologies are fully bending-dominated (Figure 2d). Although valid in many cases, the classification of cellular materials as bending- or stretching-dominated based on their topology does not account for influencing factors such as the loading conditions (Figure 2e) or the shape and rigidity of the nodes, which is of particular relevance for hollow-beam lattices. The topology of a structure may therefore not sufficiently indicate its bending-or stretching-dominated behavior.
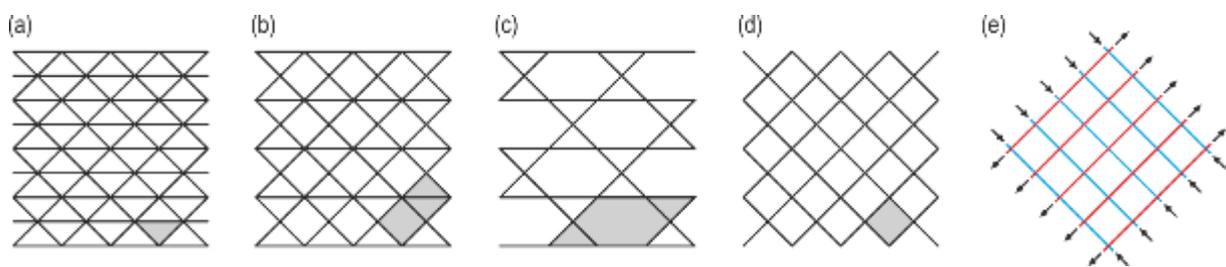

Figure 2. Bending- versus stretching-dominated behavior. (a) Stretching-dominated, rigid topology (Z=6) constructed from rigid triangular unit cells. (b-c) Periodically-rigid, theoretically stretching-dominated topologies consisting of non-rigid unit cells, (b) Z=5, and (c) Z=4. (d) Non-rigid, generally bending-dominated topology (Z=4) constructed from non-rigid unit cells. (e) Non-rigid topology which for the indicated load case behaves fully stretching-dominated representing the least weight optimum. Unit cells are shaded in gray.

Introducing *lattice architecture* into cellular materials can markedly expand the boundaries of accessible material property space, in particular in the low density regime.[49] A lattice material is defined as a periodic network of structural elements such as slender beams or rods.[49] Apart from the obvious case of lattice trusses, this definition includes shell-like designs such as honeycombs. For a lattice to be formally considered a material instead of a structure, the length scale on which a load is applied should be large compared to that of the lattice elements.[49] The most common mechanically investigated lattices are rigid assemblies of octahedron and tetrahedron unit cells, named octet-trusses (see right three structures in Figure 1).[52] Beyond high strength and stiffness at low weight[53,54], lattice architecture offers a range of other exceptional mechanical properties. Some of those properties such as tunable energy

absorption[55] can be incorporated in stretching-dominated designs. Others, including tailorable thermal expansion[56], origami-based adaptivity[57], and auxetic[58] or fluid-like behavior[59], involve hinge-like deformation and folding of bending-dominated topologies. These mechanisms are typical of mechanical metamaterials[60–62].

The behavior of *metamaterials* is determined by their topology rather than by their composition. Classically, photonic[62–64] and phononic[62,65,66] crystals derive their properties from wave phenomena and therefore strongly depend on the length scale of their patterns. Photonic crystals for optical cloaking[22] are nanolattices designed to direct light of a certain wavelength around an object rather than scattering it; this would not be possible with self-similar lattices at larger scales. By contrast, mechanical metamaterials rely on scale-independent deformation of their unit cells, and self-similar macro- and nanoscale auxetic[67] and pentamode[21,59] metamaterials have been demonstrated.[61]

Certain biological lattice architectures consist of nanoscale building blocks, allowing their mechanical properties to benefit from both optimized topology and material size effects **(Figure 3)**.[68,69] The architecture of diatoms[10,70], a common type of phytoplankton, is nanometer- or even molecular-scale and has been shown to be remarkably strong[71]. Other natural materials such as cancellous bone[72] or Euplectella glass sponges[73] have lattice elements on the scale of millimeters and are comprised of a hierarchically structured constituent material. Cancellous bone grows adaptively according to the loading situation, with the thickness and the orientation of each ligament depending on the magnitude and orientation of loading.[74,75] The resulting structure is an anisotropic network oriented in the direction of the principal tensile and compressive stresses.[75] this architecture is a classic example of a least-weight design.[76,77] Interestingly, these structures behave stretching-dominated despite not being fully triangulated because struts aligned with the principal stress direction experience no bending moment (Figure 2d).[75] Hierarchical design of a solid material from nanoscale building blocks allows for the

exploitation of extraordinary nanoscale strengths and enables high toughness at the macroscale.[68] On the lowest level of hierarchy, solid bone[72], enamel[78], and nacre[79] consist of ceramic-like elements on the order of 1-100 nm held together by a small volume fraction of a soft organic matrix.
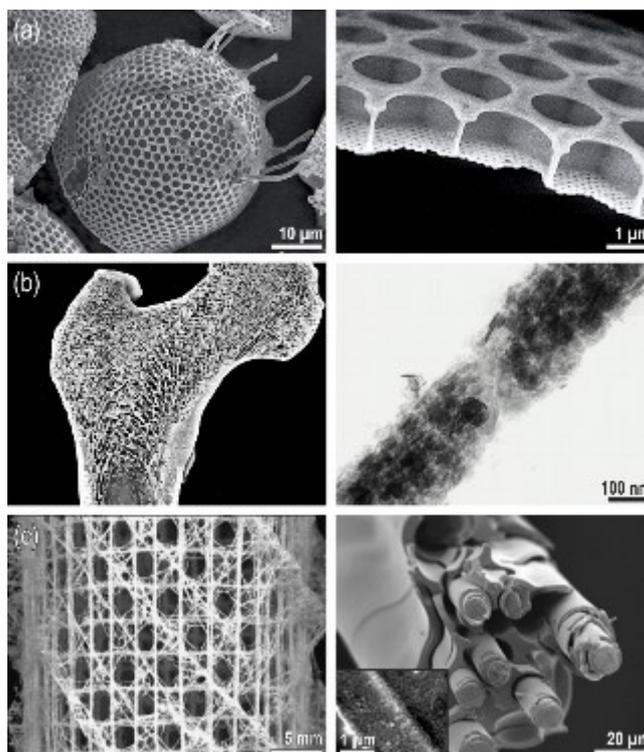

Figure 3. **Biological hierarchical lattice materials gain high mechanical robustness from optimized topologies and mechanical size effects in their nanoscale basic building blocks.** (a) Hierarchical diatom lattice comprised of nanoscale lattice elements. (b) Cancellous bone network (left) whose hierarchical solid material consists of arrays of mineralized collagen fibrils; (right) mineralized collagen fibril of a turkey tendon which is assembled from 2-4 nm thick plate-like crystals. (c) Euplectella glass sponge lattice (left) and its hierarchically structured base material with 25 nm size nanoparticles on the lowest hierarchical level. Reproduced with permission, [80] 2014, The Royal Society of Chemistry, [81] 2017, Karlsruhe Institute of Technology, [72] 1998, Annual Reviews, [73] 2005, The American Association for the Advancement of Science.

Nanolattice materials, or simply *nanolattices*, are a novel class of mechanical metamaterials; their effective properties are determined both by their topology and their nanoscale architecture, through which they are capable of exploiting unique size-affected material properties. The full potential of nanolattices is actively being discovered, and the remarkable properties that have been found to date may just be the tip of the proverbial iceberg. We still cannot mimic the

complex hierarchical architecture of biological materials, and scaling-up nanolattices for use in technological applications without sacrificing their beneficial properties will be one of the futures challenges. Prototypes of bio-inspired multi-scale lattices, up to several centimeters in size, have recently demonstrated exceptional properties[82,83] compared to their first order counterparts[13,19]. While they are still at the outset of their development, nanolattices may eventually lead us to a new era of lighter, stronger, and more durable multifunctional materials.

In this paper, we examine the unique mechanical properties of nanolattices. Key mechanisms governing the behavior are discussed in the context of lattice architecture and size-effects, and shortcomings along with potential avenues for overcoming them are identified. We examine nanolattice performance in relation to large-scale lattice materials, disordered nanoporous materials, and bulk materials to provide a comprehensive review of their materials property space. We further investigate the evolution of nanolattice materials throughout other disciplines, and discuss multifunctionality, relevant fabrication methods, up-scaling approaches, and future directions.

2. Exploiting Nanolattice Architecture

Here we discuss the benefits of combining nanomaterials and lattice architectures with a particular focus on mechanical properties. Properties unique to nanolattices are identified, and their dependence on small-scale materials effects, architecture, or a combination of the two is examined. In this context, not all lattices presented here are fully nanoscale; for properties that rely on scale-independent effects, we discuss where nanoscale structuring may be advantageous for multifunctional reasons and point out where the incorporation of material size effects has the potential to improve properties. We examine which of the presented characteristics can be successfully combined and which ones are incompatible.

2.1. Strength

The strength of a nanolattices is defined by three factors: (I) the architecture, (II) the length scale, which controls the effect of size-dependent strengthening, and (III) the solid material composition and microstructure, which correlate with the fabrication methodology.

In the context of lightweight materials design, one of the most important figures of merit to evaluate a material's performance is its specific strength, or the ratio between its strength and density. When considering specific strength, there are ultimately two necessary conditions to justify nanolattice materials and the enormous effort to process them. First, to legitimate the lattice architecture, they must achieve a combination of strength and density which may not be attained by any fully dense material. In relation to the material property space accessible by commercial bulk materials, this is often referred to as reaching the "white space". Second, nanolattice materials must capitalize on strength gains from material size effects, otherwise the same performance can be realized by self-similar macro-scale lattice materials.

2.1.1. The Strength of Existing Nano-, Micro- and Macrolattice Materials

Figure 4a shows a compressive strength versus density material property chart comparing different nano-, micro-, and macrolattices as well as stochastic nanoporous foams and commercial bulk materials. Lattices with rigid and non-rigid topologies and with different material compositions are included across all length scales. The dashed diagonal guidelines represent materials that have the same specific strength. Correspondingly, the theoretical limit bound is defined using diamond, which has the highest specific strength of all bulk materials, and graphene[44], which exhibits the highest strength measured to date.

[84]	[84]	[85]	[1]	[1]	[86]
[19]	[19]	[82]	[13]	[87]	[14]
[15–17]	[83]	[19]	[88]	[9]	[2,3]
[53]	[52]	[89]	[90]	[91,92] / [93–95]	[96]

Figure 4. Compressive strength-density materials property chart of different nano-, micro-, and macrolattices as well as stochastic nanoporous and commercial bulk materials. Symbol shapes relate to the constituent material, symbol colors indicate the length scale of structuring (fillings = feature diameter, lines = shell thickness, if any). (a) Absolute strength vs. density plot showing that many nanolattices reach far into the low-ρ-high-σ, or the ultralow-ρ "white space". (b) Strength normalized by Young's modulus vs. relative density plot, showing that nanolattice materials are capable of exploiting material strengths up to the theoretical limit ($E_s/10$), whereas the bulk material strengths are often on the order of $E_s/300$. For all structures the rigidity of the topology (r = rigid, nr = non-rigid) as well as a brief description of the applied fabrication process is given. For graphene[44] the tensile strength is shown. Images adopted from [1,14,82,83] and reproduced with permission, [84] 2016, [13,19] 2014, [15] 2011, The American Assosiation for the Advancement of Science, [9] 2017, [3] 2016, [53,89] 2015, [85] 2011, [94] 2007, [52] 2001, Elsevier, [97] 2007, [98] 1998, American Chemical Society, [87] 2016, John Wiley and Sons, [90] 2015, American Society of Mechanical Engineering, [92] 2006, Cambridge University Press.

Overall, the specific strength of the lattice materials presented here roughly increases with decreasing structural length scale. This is demonstrated using a color scale, where materials with larger features are blue and those with smaller features are red. Depending on their material composition, some of the nanolattices reach far into the chart's "white spaces". The impact of architecture is evident when comparing different carbon-based or hollow-beam nickel data, where the strength of stochastic nanoporous materials and lattices with non-rigid topologies falls short of the strength of rigidly architected lattices of similar size.

Two distinct density regimes best illustrate the enhanced performance of nanolattices. (I) In the range of 0.1-1 g/cm³, glassy carbon nanolattices[1], self-assembled core-shell silica-titania inverse opals[2,3], and core-shell polymer-alumina honeycombs[14] reach strengths of up to 400 MPa. Their strength-to-density ratios clearly outperform those of all bulk metals and alloys, polymers, technical and biological cellular materials as well as micro- and macrolattices and nanoporous foams. Glassy carbon honeycombs[1] even reach strengths above 1000 MPa, leaving diamond as the only bulk material with a notably higher ratio of strength-to-density.

13

(II) In the ultra-low density regime, below 0.01 g/cm³, hollow-beam octet lattices comprised of alumina shells on the order of 5-50 nm thickness are up to ten times lighter than the lightest technical foams yet they still achieve strength-to-density ratios comparable to wood and certain aluminum alloys.[13,82] These nanolattices are often built using multi-scale architecture[82,83] (Section 4), and they outperform other ultra-low density materials such as nanoporous silica aerogels[96] and hollow-beam nickel lattices fabricated by SPPW[15] by a factor of more than 10.

Reaching into the material property "white spaces" is not limited to nanolattices, as demonstrated by hollow-beam nickel and alumina lattices[19,83], which have notably larger dimensions than nanolattices but maintain similar or greater strengths. Any architected material made of a strong enough constituent material is capable of reaching into new material property spaces, as the diagonal guidelines in Figure 4a indicate. Nanolattices such as self-assembled nickel gyroids[9], core-shell polymer-nickel composite lattices[88] or hollow-beam gold lattices[90] have comparable or lower strengths than bulk materials of equal density despite their small dimensions.

To visualize the strength gain of nanolattice materials compared to larger-scale cellular materials and bulk solids, we normalize the data of Figure 4a with the constituent solid materials Young's moduli[3,19,51,53,84,99–101] (E_s) in Figure 4b. Core-shell composite lattices are excluded from this analysis as samples have varying constituent material ratios and therefore cannot be correlated to equivalent bulk materials. The guidelines $\left(\sigma_{eff}/E_s\right) \propto \bar{\rho}$, $\left(\sigma_{eff}/E_s\right) \propto \bar{\rho}^{1.5}$ and $\left(\sigma_{eff}/E_s\right) \propto \bar{\rho}^2$, indicate different scaling laws classically associated with stretching-, bending- and buckling governed behavior, respectively. As a point of reference, the strength of ductile bulk metals is typically on the order of $\sigma_s \sim E_s/300$[51], and brittle materials such as ceramics typically have a yield strain well below 1%[102], for which Hooke's law gives strengths on the order of $\sigma_s \sim E_s/100$.

In the range of $\bar{\rho} > 10\%$, nanolattices substantially outperform both macroscale cellular materials and the corresponding fully dense bulk solids from which they derive their properties. Glassy carbon nanolattices achieve up to 400% of the compressive strength of bulk glassy carbon[99] even though their relative density is only 10-25%. Glassy carbon honeycombs resist compressive stresses 16 times as high as the corresponding bulk material at a relative density of 44%. Self-assembled nickel gyroids reach strengths in the range of $E_s/300$ at about 40% relative density. At these high relative densities, the relative contribution of nanoscale size-effects to the strength is much greater than that from the architecture. This is best illustrated with stochastic nanoporous gold, which as well reaches strengths on the order of $E_s/300$ at relative densities of 20-40%.[93–95] Despite their rigid topology, the strength of glassy carbon and hollow-beam alumina nanolattices as well as copper microlattices scale with relative density by the power of >1.5, underperforming the prediction for stretching-dominated material strength.[1,13,89]

For lower relative densities of $\bar{\rho} \leq 1\%$ the architecture has a more significant impact on the strength and the effect of the length scale is less apparent. The strengths of both micro- and nanolattices with rigid topologies in this density regime scale linearly with the relative density, clearly outperforming lattices and nanoporous materials with non-rigid topologies. The guidelines in Figure 4b can be used to estimate that the constituent materials' strengths are approximately equal to the corresponding bulk material strength. It is noted that essentially all lattices with $\bar{\rho} \leq 1\%$ are made from hollow shells with nanoscale thickness; no macroscale lattice has been reported that is capable of achieving this scaling at ultra-light weights.

2.1.2. Architecture and Strength

The impact of architecture on the strength of a lightweight material is independent of any length scale effects. **Figure 5a** shows the ratio between ideal stretching- and bending-dominated

strength which increases exponentially with decreasing relative density. For lattices with $\bar{\rho} > 10\%$, which corresponds to the strongest nanolattices, the strength gain of stretching- compared to bending-dominated behavior is less than three; this rises to above a factor of 30 in the ultra-low density regime below $\bar{\rho} = 0.1\%$. The effective strength of cellular materials (σ_{eff}) can be approximated by the first order scaling law

$$\sigma_{eff} = C\bar{\rho}^a\sigma_s, \tag{1}$$

where σ_s is the constituent solid material strength, C is a geometric parameter, and the exponent a is 1 for stretching- and 1.5 for bending-dominated behavior.[50] For many near-isotropic cellular topologies, such as the octet lattice and open-cell foams, $C \approx 0.3$ has been found analytically and empirically.[51,52] The normalized strength of glassy carbon nanolattices with $\bar{\rho} \approx 25\%$ whose architecture is designed to be stretching-dominated is about six times higher than that of nickel gyroids of comparable relative density with a non-rigid topology (Figure 4b). Based on Figure 5a, the architecture contributes to approximately a factor of two to this strength difference, meaning a factor of three can be attributed to the difference in constituent materials. In real structures, the difference between strengths likely has a greater dependence on material compositions, meaning architecture has a less significant impact on the effective strength for high relative density materials. In contrast, rigidly designed nickel lattices with $\bar{\rho} \approx 0.3\%$[19] are 20 times stronger than those with non-rigid topologies[16]; from Equation 1, this difference is almost entirely due to the architecture.
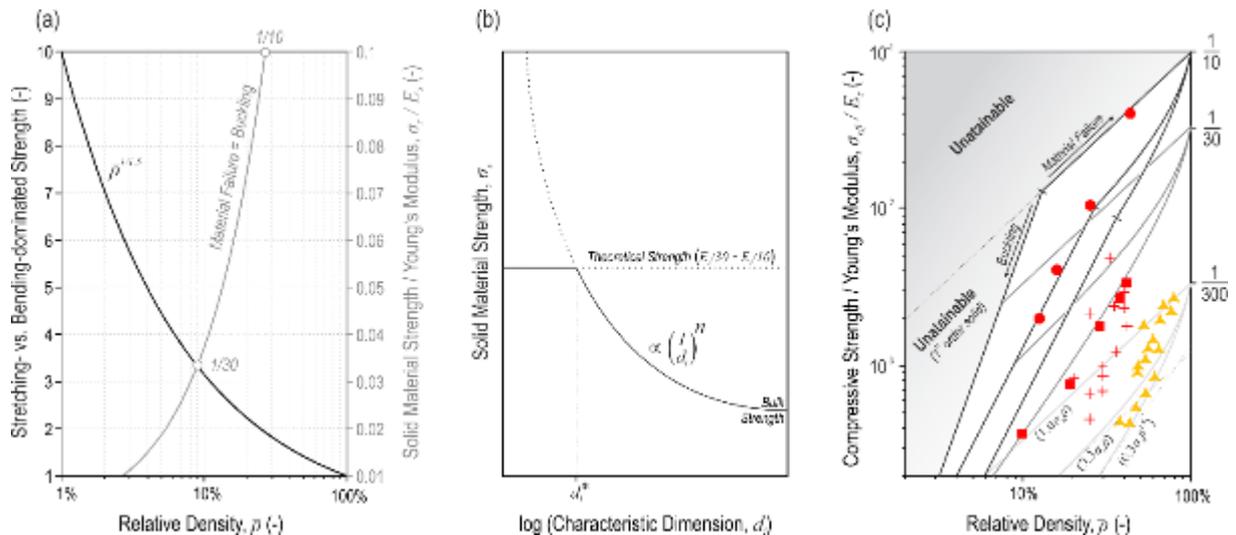
Figure 5. The impact of architecture and size effects on the strength of nanolattice materials. (a) The strength gain of stretching- over bending-dominated behavior increases exponentially with decreasing relative density *(black curve)*. Buckling before material failure becomes increasingly critical with a growing ratio of strength-to-Young's modulus (σ_s/E_s) of a lattice's solid material; the *gray curve* shows the transition between Euler beam buckling and material failure of an ideal solid beam octet lattice with rigid joints. (b) Schematic representation of size-dependent material strengthening. (c) Normalized effective strength (σ_{eff}/E_s) vs. relative density material property chart showing the interaction of size-dependent material strengthening and architectural instability. The cellular material bounds for σ_s of $E_s/300$, $E_s/30$, and $E_s/10$ are shown. See Figure 4 for data point legend.

Increasing the anisotropy of a topology can lead to a strength increase of a factor of up to three. Geometric parameters of $C > 0.3$ can be reached when lattice elements are added, removed, or varied in diameter, or when unit cells are stretched corresponding to a preferred loading direction.[14,90,103] Due to the effects of anisotropy, lattices with non-rigid designs can have strengths comparable to rigid architectures and may outperform them in some cases. For example, lattices with stretched hexagonal-prismatic unit cells were shown to have a 20% increased strength compared to regular octet lattices.[87] Values of $C = 1$ and $a = 1$ correspond to the Voigt bound (Equation 1), which represents the maximum theoretical effective strength for any cellular material. It can be achieved when the entire solid material of a structure is aligned with the direction of an applied load and therefore is stressed uniformly, such as for ideal honeycombs under out-of-plane loading or a square lattice under biaxial loading (Figure 2e). Values of $C < 1$ arise due to the misalignment of lattice elements with respect to an applied

load. In practice, bending of lattice elements, imperfections, Poisson expansion, instability effects, and experimental misalignment result in additional knockdown of this geometric prefactor.

At sufficiently low relative densities, lattice elements may be slender enough to collapse by elastic buckling before reaching the material strength. The effective strength can then be obtained by replacing σ_s in Equation 1 with the elastic buckling strength of a lattice element (σ_{eb}). The Euler buckling criterion of a slender beam is $\sigma_{eb} = k^2\pi^2 I E_s/(Al^2)$, where E_s is the Young's modulus of the solid material, I is the area moment of inertia, A is the lattice elements cross section, and l is its length.[51,53,104] The constant k depends on the boundary conditions and is equal to 2 for rigidly jointed beams and 1 for pin-jointed beams. For a honeycomb wall under out-of-plane loading, the buckling strength relationship $\sigma_{eb} = KE_sL/(1-v_s^2)$ is valid, where v_s is the Poisson's ratio of the constituent material, L is the width of the cell wall, and K is the constraint factor, which is 2 for the pin-jointed and 6.2 for the clamped case.[51,105] Correspondingly, the effective elastic buckling strength (σ_{eff}^{el}) is given by

$$\sigma_{eff}^{el} = D\bar{\rho}^b E_s \tag{2}$$

where D is a geometric parameter and the exponent b is 2 for any open-cell material[51] and 3 for honeycombs under out-of-plane loading[105]. For stochastic foams $D \approx 0.05$, and for honeycombs $D \approx 6$ has been found.[51,105] For an octet lattice with circular, rigidly connected, solid struts, a geometric parameter of $D \approx 0.123$ can be approximated.[52,53] By relating Equations 1 and 2 it is possible to find the relative density at which the failure mode switches from yielding or fracture to elastic buckling as a function of the ratio between σ_s and E_s (Figure 5a).

Material instability events like buckling are increasingly relevant for the design of nanolattices. Instability plays a role in the effective strength of a lattice when the constituent material strength

is sufficient to prevent failure before the onset of the instability. If we take $\sigma_s \approx E_s/300$, as is the case for many macroscale cellular metals and ceramics, material failure will generally occur well before the onset of any structural instabilities, meaning buckling will not play a role in the lattice strength (Figure 5a). This changes dramatically when the ratio between σ_s and E_s increases. From Equation 2, the failure of a solid-beam octet nanolattice will be governed by elastic buckling below $\bar{\rho} \approx 9\%$ when $\sigma_s = E_s/30$ and below $\bar{\rho} \approx 27\%$ when $\sigma_s = E_s/10$ (Figure 5a). Similar relationships can be found for other types of architecture. The high constituent material strength of carbon nanolattices can therefore explain the scaling behavior of their effective strength; the failure of samples with a relative density between 13% and 16% is governed by elastic buckling. Hollow-beam lattices and hierarchical architectures can have significantly improved buckling resistance, facilitating linear scaling of the strength with relative density down to 0.01% (Figure 4b). Shell buckling may still limit the strength of very thin-walled structures, as low density hollow-beam nickel octet microlattices[19] show.

As the relative density of a lattice increases beyond ~10%, its elements start to become short and squat, and the first order scaling laws in Equation 1, which are derived assuming lattices consist of slender beams, begin to break down.[51] The theoretical maximum effective strength of an isotropic cellular material can be estimated across all relative densities using the non-linear Hashin-Shtrikman (H-S) bounds[9,106] of

$$\sigma_{eff} = \frac{2\bar{\rho}}{\sqrt{4+\frac{11}{3}(1-\bar{\rho})}} \sigma_s \tag{3}$$

Below $\bar{\rho} \approx 10\%$, Equation 3 can be approximated by the first order scaling relationship in Equation 1 with values of $a = 1$ and $C \approx 0.72$. This maximum strength bound is over two times higher than the ideal relationship predicted for near isotropic lattices, though.[52] Gibson & Ashby have defined the transition between true cellular solids and solids containing isolated pores to be at $\bar{\rho} \approx 30\%$.[51] Above this relative density the non-linear H-S-bounds can be used

to explain the scaling behavior, such as of the copper octet lattices and nickel gyroids (Figure 5c).

The mechanical behavior of hollow-beam and core-shell composite lattices is not always well captured by classical lattice theory. The mechanistic underpinnings for their strength are complex and are a subject of current research. Hollow lattices are often observed to have a weaker strength than that predicted by Equation 1, and this is primarily attributed to localized bending of the hollow nodes. Strength is limited by the "weakest link", so bending of hollow nodes may not have much effect on lattices with a bending-dominated topology, as is the case for hollow-beam nickel lattices made by SPPW[15], whose effective strength scaling is well described by Equation 1. However, hollow node bending can have a drastic effect on the strength of stretching-dominated topologies. Also, high sensitivity to processing-related imperfections such as waviness and non-ideal beam cross-sections has been discussed.[13,16,19,82] The linear strength scaling observed in rigid micro- and nanolattices at low $\bar{\rho}$ is up to 10 times lower than the strength predicted by theory (Figure 4b); using Equation 1 to estimate the constituent solid material strength (σ_s) of hollow-beam alumina lattices results in values of $\sigma_s \approx E_s/300$ (Figure 4b), despite values of $\sigma_s \approx E_s/30$ having been found for single lattice elements[107].

Shape optimization of lattice nodes may have the potential to improve the strength in particular of hollow-beam and core-shell nanolattices. In core-shell lattice materials, stress concentrations were shown to increase dramatically with an increasing stiffness gradient between the core and shell, with the extreme case being a hollow shell[3,87]. For polymer-alumina core-shell lattices, stress concentrations were also shown to cause substantial knockdown of the tensile strength with respect to the compressive strength.[87] Hollow "shellular" lattices[108], namely lattices without struts that consist only of smooth interconnected nodes, were developed with the aim to reduce stress concentrations. Despite their optimized node shape, they have a fairly low

geometric parameter, C, and a high sensitivity to shell buckling instabilities, though, and show little improvement in strength with respect to non-shape-optimized hollow-beam octet lattices.[108,109]

2.1.3. Size Effects and Strength

When the length scale of architecture of a cellular material is small enough to fully exploit size-dependent strengthening, its effective strength may be on the order of 30 times higher than that of self-similar macroscale materials. A brittle perfect crystal reaches the theoretical strength (σ_{th}) when the atomic bonds of two adjacent atomic layers break simultaneously. Based on an equilibrium analysis of the work required to cleave the crystal and the energy released in the formation of the new surfaces, σ_{th} has been estimated to be on the order of $E_s/10$.[102] For ideal ductile materials, a theoretical strength of $E_s/30$ has been derived based on a shear failure criterion.[102] In practice, the synthesis of monolithic bulk materials involves the introduction of imperfections such as dislocations, grain boundaries, voids and cracks, all of which give rise to typical bulk strengths of metals and ceramics on the order of $E_s/300$. The relative strength-density property chart in Figure 5c illustrates the cellular material bounds for different ratios of σ_s to E_s.

The strength of a material depends on the characteristic intrinsic size, i.e. the length scale of its microstructure meaning the size and distribution of its flaws. Corresponding to Griffith's law[28], the fracture strength (σ_f) of brittle materials increases as

$$\sigma_f = Y \frac{K_{Ic}}{\sqrt{\pi a_c}} \tag{4}$$

when the critical size of a crack (a_c) is reduced.[102] The fracture toughness (K_{Ic}) quantifies a material's resistance to crack growth, and Y is a non-dimensional geometric parameter. In bulk technical ceramics, the size of cracks is typically on the microscale or larger, resulting in

characteristically low fracture strengths[51]. The yield strength (σ_y) of ductile metals is generally governed by the presence of obstacles to dislocation motion and may be described by

$$\sigma_y = \sigma_0 + \frac{k}{l^n} \tag{5}$$

where σ_0 usually is the bulk strength and k and n are constants.[30] The characteristic length (l) traditionally represents the size of grains or particles or the spacing between dislocations. When l is taken to be the grain size, Equation 5 is known as the Hall-Petch relation[110,111], which describes strengthening in polycrystals with decreasing grain size. In this equation, $n = 1/2$ and σ_0 is an estimate of the strength of a single crystal (for $l \to \infty$). Strengthening mechanisms like the Hall-Petch relation are well established, although the grain sizes of bulk metals are typically above the nanoscale.

Ultimately the intrinsic size of a material is limited by its extrinsic size, i.e. its characteristic dimensions (d_i). As the size of a material approaches the nanoscale, this finiteness becomes "feelable" and it can be assumed that intrinsic features are on the same length scale as extrinsic ones, i.e. a_c, $l \propto d_i$. This leads to the well-known "smaller is stronger" phenomenon[27,29–31], where strength have been found that far exceed bulk values. There is no universal scaling law for size-affected material strengthening as it arises due to the complex interaction of a number of different intrinsic and extrinsic mechanisms. Yet based on relations like those in Equations 4 and 5, the strength of both brittle and ductile solids (σ_s) is often estimated to increase as

$$\sigma_s \propto \left(\frac{1}{d_i}\right)^n \tag{6}$$

at small scales (Figure 5b), where n generally is in the range of 0.5-1[29,30].

Below a certain critical dimension (d_i^*), which is typically in the range of 1-100 nm, σ_s can reach values as high as the theoretical strength. Theoretical strength has repeatedly been demonstrated with single crystalline ceramic and metallic specimens[37], where the confined extrinsic sizes result in a near ideal material. Flaw insensitivity has also been discussed for

length scales below d_i^*.[29] According to Equation 4, the stress needed to fracture a brittle material with a critical crack length smaller than $a_c^* \propto d_i^*$ would exceed the theoretical strength. Notch insensitivity in ductile single crystalline gold nanowires has been shown to result from strain hardening.[48] No polycrystalline metals have been found that reach σ_{th}, and the critical dimension relates instead to the peak strength of the grain boundaries.[27,31,112] When dislocation loops no longer fit inside grains, grain boundary strengthening breaks down.[27] In size ranges below d_i^*, mechanisms such as sliding of grains at the free surfaces can induce a weakening effect.[27,31,113]

In a lattice, the characteristic dimension (d_i) may be the beam diameter or the wall thickness of an individual lattice element, which in a nanolattice may be designed as small as the critical dimension (d_i^*). This mechanism allows nanolattice materials to substantially exceed the limits of macroscale cellular materials, as Figure 4b and Figure 5c show. By contrast, self-similar macrolattices with $d_i \gg d_i^*$ cannot benefit from the size-affected strengthening in Equation 6.

Pyrolytically derived ceramic nanolattices exploit material strengths on the order of the theoretical strength. Figure 5c shows that the effective strength of the glassy carbon honeycombs[1] and the nanolattices with $\bar{\rho} \approx 25\%$[1] reach the cellular-materials' bounds for stretching-dominated behavior corresponding to $\sigma_s = E_s/10$ with $E_s = 28$ GPa[99]. High purity of the starting resin results in a low population of flaws after the material is transformed into a ceramic.[84] Polymer resin-derived SiOC lattices and honeycombs with macroscale dimensions already achieve remarkable strength, and when the dimensions are reduced, the flaw sizes decrease correspondingly. For a solid-beam lattice, a surface crack along the diameter of a strut may be a critical strength-limiting flaw. If a fracture strength of $\sigma_f = E_s/10$ is used, Equation 4 gives a critical flaw size of $a_c \approx 30$ nm for glassy carbon with $E_s = 28$ GPa[99], $K_{Ic} = 0.91$ MPam$^{0.5}$[114], and $Y = 1$[115]. The strut diameters of the glassy carbon nanolattices are

in the range of 200 nm, flaws are likely to be much smaller than 30 nm, and based on Equation 4 it is reasonable to expect corresponding material strengths of $E_S/10$.

Atomic layer deposited hollow-beam ceramic and core-shell composite nanolattices notably benefit from material strengthening size effects, but they may not make full use of them in their effective properties. In agreement with Equation 6 with $n = 0.5$, tensile experiments on polymer-alumina composite lattice elements[107] and bulge tests on suspended alumina membranes[100] showed that the strength of ALD alumina shells increases up to 5.5 GPa when their thickness is reduced below 50 nm. The theoretical strength of these materials has not been reached, a fact that may be attributed to the porosity of atomic layer deposited ceramics, which is as also reflected in their reduced density[116] and Young's modulus[100] compared to the corresponding bulk material. Although strengths of 5.5 GPa are below the theoretical limit, they are as much as 20 times higher than the corresponding bulk strength[51,117]. As described in Section 2.1.2, strength gains in hollow-beam and core-shell composite lattices are often not fully reflected in their effective strength due to their shell-based designs and their sensitivity to structural imperfections. The constituent material strength of sintered particle-based lattices[19] is limited by their high flaw population, which may be rather independent of the length scale.

Single crystalline metallic nanolattices achieve material strengths in the range of the theoretical shear strength. Interpolating the measured effective strength of the nickel gyroids[9] to that of the fully dense material gives $\sigma_s = E_s/30$ with $E_s = 214$ GPa[51] (Figure 5c). Nickel gyroid films have a columnar polycrystalline structure with in-plane grain sizes of about 1.5 μm. However, their constituent unit cell sizes of 45 nm enable strengths on the order of single crystalline nickel. Nanoscale single crystalline metal specimens approach theoretical strengths via mechanisms such as dislocation starvation, wherein dislocations exit at free surfaces and leave behind a dislocation-free material.[31] The critical dimension of face-centered cubic nickel can be estimated to be 13nm using Equation 5 with k estimated from the Burger's vector and the shear

modulus and $n = 0.66$[118]; this matches the strut diameter of the nickel gyroids.[9] Similar relations can be found for nanoporous gold foams, whose effective strength has been described over a feature length scale range of 10-900 nm by replacing σ_s in Equation 1 with Equation 5;[94] comparable systematic studies have not yet been performed for nanolattices.

The benefit of small-scale structuring may be limited in lattices made from polycrystalline metals. The strength of electroless deposited nanocrystalline nickel-based thin films, similar to those used in some hollow-beam microlattices[15,19,83], has been estimated to be ~2 GPa based on hardness measurements.[19,101] While this strength is higher than many bulk nickel alloys, strengths of 4.3 GPa have been found in amorphous metal films of core-shell composite lattices[88]. Compression tests of 7 nm-grained hollow-beam lattice elements showed a drastic decrease in strength when wall thicknesses were reduced from 500 nm to 150 nm, the magnitude of which could not be explained by geometry alone and was also attributed to the "smaller is weaker" effect that is induced by the sliding of grains at the free surfaces.[101] A similar behavior may explain the drop in strength of hollow-beam nickel octet microlattices[19] shown in Figure 4. As dimensions are reduced, the fraction of grains at the free surfaces increases, intensifying surface sliding weakening effects. This is distinctly reflected in low-strength hollow-beam gold lattices synthesized via sputtering[90], which have grain sizes of 25-50 nm and feature dimensions down to 200 nm. Copper microlattices with strut diameters in the range of 1-3 μm mostly consist of grains spanning entire lattice members[89]. They are therefore neither fully single- nor polycrystalline, and corresponding strengthening and weakening effects may be present at the same time. The constituent material strengths of copper microlattices can be estimated to be on the order of $E_s/300$. However, their effective strength has been shown to be three times higher than the strength of 10 μm thick polycrystalline copper films synthesized under identical conditions.[89]

2.2. Stiffness

In quantifying the performance of lightweight materials, the specific stiffness, or the ratio between Young's modulus and density, is as important as the specific strength. Lattice stiffness depends on architecture, and topologies that are optimized for high strength generally achieve high stiffness. In contrast to strength, reducing the length scale of lattice architectures has not been shown to lead to any size-affected increase in the stiffness of the constituent materials. Size-effects in the stiffness are still a subject of current research and may be limited to a small number of materials, such as carbon[43–47]. Taking advantage of stiffness size effects in nanolattices may require a further decrease in feature sizes beyond what is achievable today.

Despite a lack of size-affected benefit to their constituent stiffness, micro- and nanolattices have pioneered new regimes of stiffness versus density material property space. **Figure 6** compares different nano-, micro- and macrolattices, stochastic nanoporous foams and commercial bulk materials. Rigid architectures of hollow-beam alumina[13,19,82] and nickel-based[19] nano- and microolattices populate the ultra-light density "white space" below 0.01 g/cm³. These materials have specific stiffnesses that do not considerably degrade over several orders of magnitude decrease in density. As a result, they substantially outperform non-rigid lattices of the same density and are demonstrably less dense than stochastic cellular materials of comparable stiffness. Ultralight micro- and nanolattices achieve new material property spaces for both stiffness and strength, but in higher density regimes of 0.1-1 g/cm³, the stiffness of nanolattices does not reach the same "white space" that is reached for strength[1–3,14]. This illustrates the beneficial impact of size-effects on nanolattice strength and its corresponding absence in the stiffness.

Figure 6. Compressive stiffness vs. density materials property chart comparing different nano-, micro-, and macrolattices as well as stochastic nanoporous and commercial bulk materials. Certain hollow-beam micro- and nanolattices reach far into the chart's ultralow-ρ "white space". For graphene[44] the tensile stiffness is shown. See Figure 4 for data point legend.

Analogously to the strength, the effective stiffness of cellular materials (E_{eff}) versus relative density is classically modeled by the relationship

$$E_{eff} = F\bar{\rho}^g E_s \tag{7}$$

where E_s is the constituent solid material's Young's modulus, F is a geometric parameter, and $g = 1$ and 2 are the exponents for ideal stretching- and bending-dominated behavior respectively. The impact of bending on the stiffness is more pronounced than it is for the strength, which has a scaling exponent of $a = 1.5$ for bending-dominated behavior. In the ultra-light density regime, stochastic materials can have scaling exponents of $g = 3$.[119] Geometric

parameters for open-cell foams of $F \approx 1$ have been found[51], and for the octet lattice, $F = 1/9 - 1/5$ has been predicted mathematically[52] depending on the loading direction. As is the case for the strength, anisotropy can lead to increased stiffness in a preferred loading direction but at the cost of decreased stiffness in other directions.

It can be seen in Figure 6 that the stiffness of many of the lattice materials does not scale perfectly linear or quadratic with the density, but instead falls somewhere in between. This occurs because the relationship defined in Equation 7 is only valid for lattices with slender beams. Equation 7 provides a useful guideline for quantifying the performance of a given topology, but it likely obscures some of the more complex mechanical phenomena observed in actual lattices, particularly in those made from hollow beams or shells. The stiffness of lattices can also be affected by structural defects like the removal of strut members, stress concentrations at nodes, local shearing and bending in strut members, and waviness or misalignment of the struts;[13,19] investigations into these effects are a topic of ongoing research.

2.3. Recoverability, Energy Absorption & Damage Tolerance

The deformability of materials can be greatly enhanced through the addition of architecture. Micro- and nanolattices are able to take intrinsically brittle and low elastic limit materials – like ceramics and certain classes of metals – and use them to create metamaterials that are able to undergo large deformations of up to 80% compressive strain without catastrophic failure.[13,15,18,82,83] This is primarily enabled by scale-independent architectures that deform in ways that accommodate large displacements and in part because of nanoscale constituent materials that can withstand larger elastic strains due to increased yield strengths. Enhancing the deformability gives rise to three important architected material properties: recoverability, energy absorption, and damage tolerance.

Hollow-beam micro-[15,18] and nanolattices[13,82] made from both ductile and brittle constituent materials have demonstrated near 100% recoverability after compression to 50% strain **(Figure 7)**. A transition from brittle failure to recoverable deformation was observed below a certain critical wall-thickness-to-strut-diameter ratio (*t/D*). This phenomenon was attributed to shell buckling of thin-walled struts, which can form low stress hinges that prevent catastrophic failure and accommodate large macroscopic reversible strain.[13,17,18] Recoverability has been shown with both rigid and non-rigid topologies, but relative densities are generally required to be very low to enable shell buckling.
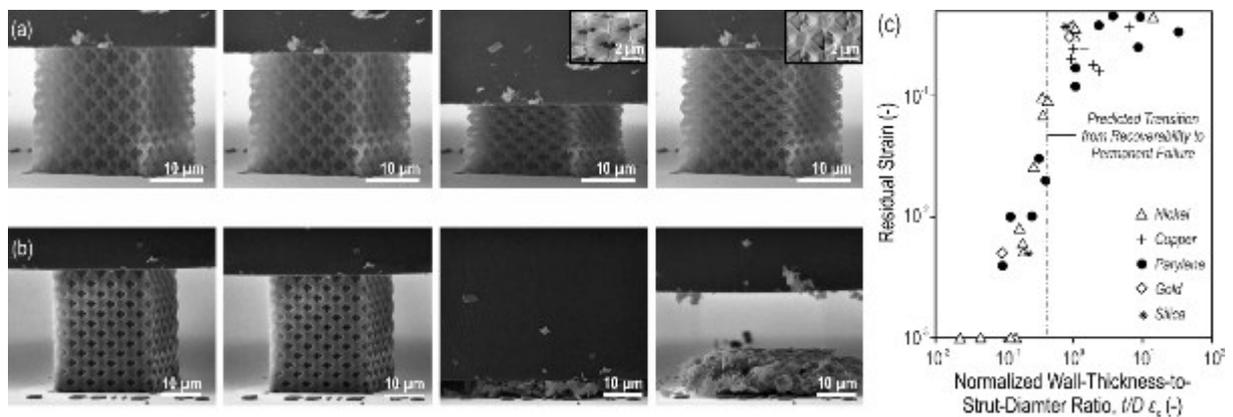
Figure 7. Recoverability of micro- and nanolattices. (a) Compression of thin-walled and (b) thick-walled hollow-beam alumina nanolattices, demonstrating the effect of shell buckling on increasing the deformability and recoverability of intrinsically brittle materials. (c) Residual strain of hollow-beam microlattices fabricated via SPPW, after 50% compression vs. wall-thickness-to-strut-diameter ratio (t/D) normalized by the yield strain of the constituent material. The critical ratio t/D that guarantees full recoverability from any imposed macroscopic strain can be estimated analytically. Adopted from [18] and reproduced with permission, [13] 2014, The American Assosiation for the Advancement of Science.

Controlling the activation of different failure mechanisms is key to enabling the enhanced deformability observed in nano- and microlattice materials. In a lattice the primary failure mechanisms are constituent material failure, beam buckling, and shell buckling in lattices with hollow members. The strength of the solid material (σ_s) is an intrinsic material property, but it can be greatly affected by feature size, as is discussed in Section 2.1.3. The beam buckling strength was defined in Section 2.1.2 for slender beams using the Euler buckling criterion of $\sigma_{eb} = k^2\pi^2 IE_s/(Al^2)$. The shell buckling strength for hollow circular beams is $\sigma_{sb} =$

$E_s(t/R)/\sqrt{3(1-v^2)}$, where t is the wall thickness, R is the beam radius, and v is the constituent material Poisson's ratio.[120]

The failure mechanism that governs the initiation of failure can be determined by setting these three equations equal. The critical transitions ratios between material failure and beam buckling, material failure and shell buckling, and beam and shell buckling for a thin walled hollow circular beam respectively are

$$\left(\frac{R}{l}\right)_{s \to eb} = \frac{1}{\pi}\sqrt{\frac{\sigma_s}{2E_s}}$$

$$\left(\frac{t}{R}\right)_{s \to sb} = \frac{\sigma_s}{E_s}\sqrt{3(1-v^2)}$$

$$\left(\frac{tl^2}{R^3}\right)_{sb \to eb} = 2\pi^2\sqrt{3(1-v^2)}$$

Using these relationships as guidelines, architected materials can be designed to undergo failure via one of these mechanisms using any constituent material.

Buckling is the cornerstone of much of the deformability, recoverability and energy absorption observed in micro- and nanolattices. It is an intrinsically elastic phenomenon, meaning that if the stress in a post-buckled beam doesn't reach the yield or fracture strength of the material, a structure will be able to recover to its original shape. This recovery can occur independently of architecture, and lattices can simultaneously be designed to be recoverable and to have high strength and stiffness.

In lattices with beam buckling dominated failure, beams must be highly slender and nodes must either be reinforced or able to rotate in order to ensure post-failure recoverability. Node reinforcement, such as selectively increasing the material thickness at the node, can be done in any architecture, but node rotation is best enabled in architectures with non-rigid topologies like octahedral-type unit cells[121], which have intrinsic mechanisms that allow for a greater

degree of deformation. In lattices with shell buckling dominated failure, shell walls must be thin and have large radii of curvature to improve structure recovery. In locally buckled sections of beams, a compliant hinge is formed that enables greater deformation.[13,55] Permanent failure can and does often occur in these locally buckled regions, but structures can still globally recover if the failure is unable to propagate to the rest of the beam. This behavior has been observed experimentally, but there is not a well-developed theory on how to design geometries that form buckled hinges that can impede brittle failure propagation.

The ability of a recovered structure to retain its initial strength and stiffness is crucial to its utility as an engineering material. Due to the activation of certain failure modes and the buildup of local damage, the post-yield stiffness and strength of a recovered structure is generally lower than that of the undeformed material.[15,55,82] Reducing the applied strain on a structure can help it to retain its strength, but it is difficult to completely preserve the initial mechanical properties. When repeatedly compressed to the same strain, structures often exhibit a stable cyclic behavior.[15,55,82] This occurs because failure modes that were activated in the initial cycle can be reactivated, minimizing the accumulation of additional damage.

Fracture, plastic work, and intrinsic material damping dissipate energy in continuum materials; in recoverable lattices, buckling and other hysteretic instabilities are the dominant mechanisms that cause energy dissipation. Beams that buckle often exhibit a bistable behavior, during deformation they undergo a snap-through between a buckled and unbuckled state. This snap-through event induces high-frequency vibrations which are eventually damped, resulting in energy dissipation. The character of the snap-through events can also be controlled by changing the type of buckling; for example, Euler buckled beams in uniaxial compression will maintain an approximately constant load, while shell buckled beams will have a drop in load carrying capacity in their post-buckled configuration.[122] In lattice architectures buckling and snap-through events can be coordinated to dissipate energy in a controlled manner, and structures

can be designed to enable layer-by-layer deformation, uniform crushing, or localized failure.[13,82,83,123–126] One important characteristic damping parameter is the mechanical loss coefficient, defined as $\eta = \Delta U/2\pi U$, where U is the stored elastic strain energy and ΔU is the dissipated strain energy.[127] It has been shown that that lattices can be designed to have exceptionally high damping figures of merit $E^{1/3}\eta/\rho$.[55] Structures with optimized damping will generally have low relative densities ($\bar{\rho} < 0.1\%$) and hence low strength and stiffness. High density architected materials that dissipate energy via snap-through buckling of hinges while maintaining recoverability have been proposed.[123–126]

When maximizing energy dissipation per unit mass, e.g. for the development of armor systems, plastic flow is the mechanism of choice. Polymer and ceramic-polymer composite nanolattices fabricated by interference lithography[62] were shown to dissipate exceptional amounts of energy per unit mass.[128–131] This was attributed to the ability of the structure spread plastic deformation over a large volume; in a bulk material, failure is generally localized to a single shear band or necking region, whereas failure in lattices can occur homogeneously throughout a sample. Although plastically deformable nanolattices possess exceptionally high specific energy dissipation, their deformation is not recoverable and therefore not repeatable.

The design of damage tolerant and lightweight materials is still a major engineering challenge. The fracture toughness of a periodic lattice scales with the square root of the unit cell size, meaning that it decreases when the unit cell size is reduced.[49,132–134] For octet or hexagonal lattices, a single "missing" beam introduces a stress concentration.[132,134] In contrast, Kagome lattices are insensitive to flaws smaller than a certain transition length.[132,135] This transition length scales with $1/\bar{\rho}$ and can be several times the unit cell size.[132] In nanolattices, material strengthening size effects should counteract the size-dependent weakening of the architecture.[134] Therefore, there may be a slight benefit to the toughness of nanolattices, but the substantial design challenge remains. A possible solution might be in the use of hierarchical

designs, where larger unit cells could impart toughness while smaller nested unit cells would be used to exploit size-dependent strengthening effects. Hierarchical micro- and nanolattices have also been observed to have increased recovery beyond that of simple periodic lattices because failure is localized to sections of hierarchical beams, allowing structures to undergo permanent damage while still recovering globally.[82,83]

There are many other size-affected material properties like enhanced ductility[38,42], fatigue resistance[136], and fracture toughness[29] that have been observed in nanomaterials but have not been used in practical implementations. Future developments in nanoarchitected material design may rely on these and other size affected material properties to push the limits of mechanical performance.

2.4. Auxetic Behavior

The concept of auxetics[137], namely materials with negative Poisson's ratio, holds great promise for adding new functionality to nanolattices. At the macroscale, auxetic structural designs are progressively employed in the development of novel products, especially in the fields of intelligent expandable actuators, shape morphing structures, and minimally invasive implantable devices.[138] There is a wealth of possible auxetic designs, many of which rely on folding and unfolding mechanisms of non-rigid topologies, and there are many possibilities for the creation of three-dimensional architectures that achieve Poisson's ratios down to -1 or lower.[139] Poisson's ratio of zero describes a material that retains its lateral dimensions upon compression, while Poisson's ratio of -1 describes a material that will shrink laterally an equal amount to what it is compressed vertically, thereby keeping its shape but not its volume. Poisson's ratios of -0.8 have been demonstrated for macroscopic lattices, and a design for an ideal dilational metamaterial with Poisson's ratio of -1 has been proposed.[67] Materials with Poisson's ratios of -1 require infinitesimal joints to achieve their performance. The small dimensions and enhanced material properties of nanolattices may be able to replicate such ideal

joints.[67] Auxetic lattices based on the bow-tie design were created **(Figure 8a-b)** exhibiting

different Poisson's ratios depending on the precise shape of their bow-tie elements.[20] In these

materials, subtle design changes were used to shift Poisson's ratio from negative to zero or even

positive values. Applying thin alumina coatings using atomic layer deposition to the polymer

structures increased the stiffness while leaving Poisson's ratio unaffected. With the ever

increasing precision in manufacturing capabilities, progressive size reduction of auxetic

geometries may allow the exploitation of mechanical size effects in nanolattice materials with

tailorable adaptivity.[140]
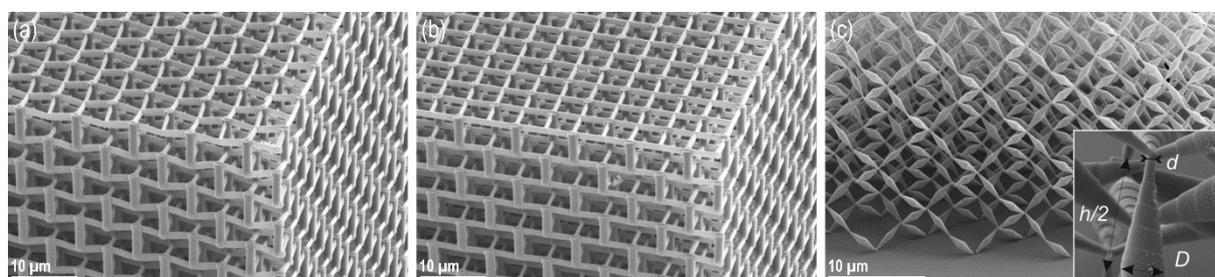
Figure 8. Nanolattices achieving extreme tunable mechanical properties. (a-b) Auxetic lattices based on the bow-tie design with four-fold symmetry, subtle structural variation changes Poisson's ratio from (a) -0.14 to (b) 0.01. (c) Pentamode lattices have a very large bulk modulus compared to the shear modulus. Ideally, the connecting points of the double-cones would be infinitely small and control the modulus ratio. Minimum cone diameters d of 550 nm were achieved. By increasing the cone diameter D, the mass density of the lattice can be adjusted. Reproduced with permission, [20] 2012, John Wiley and Sons, [21] 2012, AIP Publishing LLC.

2.5. Metafluidic Behavior

Pentamode metamaterials, also referred to as metafluids, have a very large bulk modulus

compared to their shear modulus, which ideally is zero. A material with a very large bulk

modulus will have little volume change during deformation, meaning its Poisson's ratio is close

to 0.5.[21] A material with a very small shear modulus will "flow away" under shear in a manner

similar to a fluid.[21] Pentamode metamaterials combine these two principles to generate an

elasticity tensor with only one non-zero eigenvalue and five eigenvalues that are negligibly

small.[60] Based on a concept by Milton and Cherkaev[141], these materials can be created using

rigid, double-cone elements connected to each other at their point-like tips and arranged in a diamond-type lattice (Figure 8c).[21] Actual structures are approximations of the ideal pentamode material having zero diameter of the cone ends, but minimum cone tip diameters of 550 nm have been achieved, resulting in bulk-to-shear modulus ratios of approximately 1000.[21] The bulk modulus of such a double-cone lattice is mainly determined by the diameter of the cone tip; increasing the cone diameter will primarily affect the mass density of the lattice and has less significance for the modulus.[142] If minimum cone diameters smaller than 550 nm were achieved, a further enhancement of the bulk-to-shear modulus ratio should be possible, which would facilitate the fabrication of three-dimensional transformation-elastodynamic architectures[21,143] like free-space cloaks that render objects invisible to incident radiation. For elastomechanical cloaking, macroscale pentamode lattices with different modulus ratios were combined to render a physical object "unfeelable".[144] The concept of reducing the dimensions of the connection points in a lattice was applied to design nanolattices with maximized anisotropy of the elastic modulus.[145] These face-centered cubic nanolattices were created using interference lithography and achieved an elastic-to-shear-modulus-ratio of four.

2.6. Non-Mechanical Properties & Multifunctionality

Photonic metamaterials[62–64] are micro- or nanoarchitected to enable interaction with electromagnetic waves such as visible light (wavelength 400-700 nm). Notable examples include silicon woodpile lattices with engineered defects exhibiting near-infrared complete photonic bandgaps, chiral and bi-chiral polymeric photonic crystals featuring polarization stopbands, photonic quasicrystals, and polymeric woodpile lattices with spatially tailored density, providing invisibility cloaking at optical wavelengths[22,23]. The development of tailored photoresists for multi-photon lithography and multi-laser polymerization approaches based on stimulated emission depletion (STED) achieve significantly increased resolution,[146–148] further enhancing the opportunity to design nanolattices with unique optical properties.

Phononic metamaterials[62,65,66] are designed to interact with mechanical waves. Mechanical waves travel within a homogeneous and isotropic medium with the dispersion relation $\omega = c \cdot k$, where ω is the frequency, k is the wave vector and c is the velocity of propagation in longitudinal or shear direction. If the medium has an intrinsic periodicity, though, a much more complex dispersion relation results, with several acoustic and optical branches. When properly designed, the periodic medium might exhibit "band gaps", i.e. ranges of frequency where wave propagation is prohibited along any direction. Acoustic metamaterials with unit cells in the centimeter range have been developed extensively.[149] Recently, DLW has been employed to fabricate phononic crystal at the microscale, which can tailor ultrasonic wave propagation.[150] Phonons (thermal vibration within the atomic lattice) are largely responsible for heat conduction in non-metallic solids. In principle, nano-architected materials could be designed to interact destructively with phonons, possibly resulting in exceptionally low thermal conductivity; the key challenge is that phonons responsible for heat conduction have extremely low wave length, and hence can only interact with architected materials with periodicity on the order of ~1 nm.[66]

Cellular materials have been exploited for *thermal management* for decades.[51,151] When fabricated in ceramic constituent at very low density, they provide exceptionally low thermal conductivity and diffusivity; conversely, when fabricated in metal with open porosity, they enable active cooling and efficient heat transfer from the hot to the cold side.[152] Optimized lattice architectures such as multi-scale heat pipe structures[153] substantially improve thermal properties compared to stochastic foams.[154] In all these applications, length scale reduction promises performance improvements, thanks to size effects in the thermal conductivity[32,33].[155]

Lattice materials with *tunable thermal expansion* can be designed by properly combining different constituent materials, or folding mechanisms similar to those of auxetic structures. A number of possible designs have been proposed and demonstrated at the macroscale.[56,156–158]

If fabricated at smaller scale, these multi-constituent architected materials would be useful for applications where dimensional accuracy is essential under continuous temperature excursions, e.g. positioning of micromirrors[159] in space applications. Recently, multimaterial PμSL has been used to develop a bi-material negative Coefficient of Thermal Expansion polymeric lattice with unit cell size of ~5mm.[160] In the context of thermal size effects, the ability to generate similar multi-material topologies with dimension reduced by several orders of magnitude may hold opportunities for novel applications.

Electrochemical phenomena such as upon lithiation/delithiation of electrodes for advanced lithium ion batteries require very large surface area, interconnected porosity, and the ability to accommodate strains, up to several hundred percent, without mechanical failure. The ability to optimize the topology of a nanolattice can dramatically improve the combination of transport, electrochemical and mechanical properties over that of state-of-the-art stochastic porous materials. Self-assembly has been applied to develop energy storage and conversion devices such as solar cells, batteries, and fuel cells.[161] Glassy carbon[162] and copper-silicon[163] nanolattices fabricated by interference lithography and DLW, respectively, were proposed as electrode materials. Although not quite a nanolattice, pillared graphene nanostructures have been shown to possess excellent specific capacitance and coulombic efficiency which are ideal properties for supercapacitors.[164]

In *bio-technology*, micro- and nanolattices with controlled three-dimensional architecture have been successfully used for tissue engineering,[165] as scaffolds for controlled cell cultures,[166] and in minimally invasive medicine[167]. Chemical functionalization, as demonstrated with polymeric lattices generated using DLW, with pre-functionalized photomonomers[168] potentially qualifies nanolattices for a variety of biomedical and biochemical applications.

3. Fabrication

Lattice structures with millimeter to centimeter scale periodicity can be efficiently fabricated via the assembly of folded and/or slotted thin sheets (similar to a cardboard box), or by modular assembly methods such as wire layup.[169] Additive manufacturing (AM) technologies[170] like selective laser sintering, selective laser melting, stereolithography and electron beam melting offer sub-millimeter resolution and increased design freedom, but at the cost of a lower production rate. The production rate of a manufacturing process generally scales inversely with its accuracy and resolution capacity. Fabrication techniques with micrometer and nanometer resolution, such as those required for fabricating nanolattices, are currently limited to a number of polymer-based, low throughput, AM and self-assembly techniques. Those that have been most successfully applied to micro- and nanolattice fabrication are described in the following sections. We discuss the achievable resolution, productivity and design freedom, and give an overview on the most commonly used methods to convert polymeric structures into ceramic, metallic and composite lattices.

3.1. Self-Propagating Photopolymer Waveguides (SPPW)

SPPW is an angled exposure technique to fabricate open-cell polymer structures from self-propagating photopolymer waveguides.[4,121] With this technique, exposes a photomonomer by ultraviolet (UV) light passed through a two-dimensional mask with a pattern of apertures as shown in **Figure 9a**. In the photomonomer, self-propagating photopolymer waveguides develop at each aperture in the direction of the UV collimated beam and cross at points of intersection, forming a three-dimensional interconnected array of polymer struts. After removing the uncured monomer, an open-cell polymer material is left behind. SPPW controls the architectural features of the bulk cellular material by controlling the strut angle, diameter, and three-dimensional spatial location during fabrication. The unit cell architecture is governed by the pattern of circular apertures on the mask and the orientation and angle on the collimated incident UV light beams. With standard UV exposure capabilities, lattices have been fabricated

with strut diameters ranging from ~10 μm to >1 mm and a relative densities between ~5 % and 30%. The overall material thicknesses can range from 100 μm to over 25 mm per exposure. The maximum achievable material thickness, which is dependent on the distance the waveguide can propagate, is roughly 100 times the lattice member diameter. To achieve higher thicknesses, multiple layers have to be exposed similar to other layer-by-layer AM techniques. The lattice strut angle relative to the exposure plane can be between ~50° to 65° for directly intersecting waveguides. Vertical or near vertical struts are also producible. Changing the aperture spacing and diameter on the mask enables variations in the lattice feature dimensions and unit cell sizes (Figure 9a). SPPW can only be used to fabricate architectures that are linear extensions of the mask; this allows a range of non-rigid lattice truss topologies and honeycombs, but prohibits rigid lattice topologies with struts parallel to the mask plane. Masks with larger apertures can be used to make negative templates for shellular topologies that are rigid and don't contain in-plane elements.[108] The main advantage of SPPW compared to other high resolution AM approaches is the substantially higher speed and scalability. 30 cm x 30 cm x 20 mm polymer lattices have been fabricated in 1 minute, and rates of more than 1 m^2/min are achievable with a continuous SPPW process. Interference lithography[62] and other angled exposure techniques such as x-ray lithography can be used to create similar topologies to those made using SPPW and with feature diameters below 100 nm, albeit at the cost of considerably lower scalability.[130] Multi-beam interference lithography markedly extends the variety of topologies that can be created.[62] A range of resin systems are available for SPPW that enable lattices from stiff,[121] viscoelastic,[171] or pre-ceramic[84] polymers.

3.2. Projection Micro-Stereolithography (PµSL)

Projection micro-stereolithography a layer-by-layer process for the fabrication of three-dimensional polymer microstructures (Figure 9b).[5] For each layer, a reconfigurable digital mask and a UV light-emitting diode (LED) array project an image onto the surface of a liquid

photomonomer bath, inducing polymerization in the shape of the projected image. The thickness of the resulting layer is in the range of 10-100 μm, depending on the penetration depth of the light, which is controlled by process parameters including light intensity[5,172,173], exposure time[172,174], and the concentration of photoabsorber[175,176] and photoinitiator[177] in the photomonomer. Lowering the polymerized layer into the resin bath forms a new liquid layer on top of the polymerized layer and the process is repeated until the desired object is completed. The spatial light modulator (SLM), which is usually a deformable mirror array (DMD), combined with projection optics defines the resolution and scalability. For example, a typical SLM with 1920 × 1080 pixels projected over an area of 15.36 mm x 8.64 mm combined with UV reduction optics with a reduction factor of 6:1 gives a final resolution of 1.3 μm/pixel at the projection focal plane. Three-dimensional lattices with feature sizes of 5 μm and 300 μm can be fabricated in areas of 1 mm and 5 cm in 1 to 2 hours, respectively. Further extending the scalability, Large Area PμSL[83] combines an addressable SLM with a galvanometric mirror scanning system to produce microscale architectures over a large area. As the light is scanned, the image projected from the SLM changes corresponding to the respective location of the pattern. Hierarchical lattice materials with over 60,000 octet unit cells and with feature sizes <5 μm (see Section 4) can be fabricated with a speed of 1,200 mm³/hour. The main advantage of PμSL compared to high resolution AM techniques such as DLW is the increased fabrication speed, which, due to the projection technique, is not compromised as feature complexity increases. PμSL can work with a range of resins with inorganic nanoparticles[178,179], pre-ceramic polymers[180–182], as well as resins with different colors[183], stiffness[184], and viscosities[185]. Multi-material PμSL with feature sizes in the millimeter range has also been shown.[160]

3.3. Direct Laser Writing (DLW)

Direct laser writing (DLW) is a multi-photon lithography process that facilitates the fabrication of fully three-dimensional polymeric micro- and nano-structures (Figure 9c).[6,7] In DLW, an optical microscope focuses a laser beam with a wavelength (λ) of typically 780 nm into a volume of liquid photoresist. The photoresist contains a photoinitiator that absorbs the laser light and causes polymerization of its monomers. The photoinitiator is transparent to light with a wavelength λ but absorbs light at $\lambda/2$, which has double the energy than light at λ. If two or more photons of wavelength λ are absorbed simultaneously, the sum of their energy is high enough to induce polymerization. This is known as multi-photon absorption, which is a second-order process that is several orders of magnitude weaker than the single-photon absorption used in SPPW or PμSL. In the DLW process, multi-photon polymerization is achieved by focusing of the laser light. As the absorption reaction depends on the square of the light intensity there is no polymerization along the path of the light but only in a small focus volume. The result is an ellipsoidal polymerized voxel, or volume pixel, that is typically >200 nm wide and >600 nm high.[148] DLW with resolutions down to 100 nm have been achieved using more complex optical configurations.[148,186] By moving the laser focus sample one can "write" three-dimensional structures into the photoresist. Piezoelectric xzy-stages with nanometer accuracy can move the sample in all directions at speeds of tens of micrometers per second. Galvo mirrors enable rapid in-plane scanning of the laser focus with a scan speed of up to m/s. In practice, both writing methods are combined to achieve typical writing speeds on the order of mm/s. The working area of both writing methods is generally limited to a few hundred micrometers, the fabrication of larger structures requires stitching of multiple writing fields. A range of positive[24] and negative[64,166,168,187,188] tone photoresists can be used in fabricating nanolattices.[189] After samples are written, the remaining photomonomer is dissolved in a developing bath, leaving the finished structure behind. Super critical drying[190] can be applied during the development stage to avoid distortion of the structure due to capillary effects. DLW has the highest achievable resolution of any fully three-dimensional AM technique, and it is

therefore the method of choice for the fabrication of nanolattices. The main challenge DLW faces is its scalability; the size of fabricated samples typically ranges from hundreds of micrometers to centimeters depending on the complexity of the structures being written.

3.4. Self-Assembly

Self-assembly based approaches have shown great promise for the fabrication of complex micro- and nanostructures, and are therefore often seen as an alternative to additive manufacturing. As defined by Whitesides and Grzybowski, "Self-assembly is the autonomous organization of components into patterns or structures without human intervention"; this process is applicable at all length scales, although the first studies focused on the self-assembly of molecules.[191]

Block copolymer self-assembly (Figure 9d) has been successfully used in the fabrication of a variety of periodic functional nanostructures with dimensions on the order of tens of nanometers.[192,193] Block copolymers are macromolecules that form separate distinct domains based on microphase separation of their constituent polymer blocks. Depending on the molecular weights and the relative compositions of the copolymer, different nanodomain structures develop. A variety of three-dimensional morphologies can be assembled.[194] Electroplating can be used in combination with self-assembled polymer templates to fabricate nanolattices from several inorganic materials. For example, three dimensionally periodic double-gyroids were fabricated with block copolymers and coated with nickel using electroplating; after removing the block copolymer, the resulting structure was a periodic double-gyroid nickel replica with strut sizes of 13 nm and a relative density of 38%.[9] Vanadium pentoxide gyroid structures were fabricated using a similar process and with strut sizes of only 10 nm.[195] Room-temperature oxidation of silicon containing triblock copolymers was shown to create silicon oxycarbide inverse double gyroids with strut sizes of ~20 nm.[196]

The self-assembly of colloidal crystals using nanoscale particles is another approach for the production of templates for ordered nanoporous structures. Inverse opals made using materials such as silica, nickel and alumina have been reported.[2,197] Typical pore sizes are in the range of a few hundreds of nanometers[2,197,198] and strut thicknesses are on the order of 100 nm[2,197]. The technological potential of colloidal self-assembly for large area fabrication has been demonstrated using nickel inverse opals that were fabricated covering 2 cm^2 areas.[197] Inverse opals are open-cell structures, when close-packed colloidal spheres are used as a template. Closed-cell structures can be produced using a colloidal crystal template composed of close packed core–shell spheres that have been infiltrated with a precursor fluid.[199] In a process similar to nanocasting[200], the precursor is converted into the target material and replicates the templated nanomorphology after the chemical removal of the hard template. Colloidal crystals made from carbon and silica and from silica spheres have been identified as the most promising template materials.[200] While colloidal crystals from monodisperse spheres have a limited range of crystal structures, binary mixtures of differently sized colloidal particles were demonstrated to form more complex topologies.[201,202]

Three-dimensional assembly of graphene and carbon nanotubes have been predicted by molecular dynamic simulations to possess a number of outstanding physical properties including mechanical, electrical, and chemical.[203–206] Synthesis of nanostructures such as pillared graphene has been shown,[207] but their structural order is limited and they generally do not possess a truly periodic architecture.

The application of self-assembly processes to the controlled fabrication of nanolattices is still in its infancy, but their implementation has great potential benefits for upscaling and mass fabrication. The two main advantages of self-assembly methods are their low-cost of synthesis and their rapid processing times. The disadvantages are the limited topological diversity and the emergence of larger-scale defects that typically propagate through the entire material; these

both need to be explored in more detail for self-assembly methods to be a truly effective
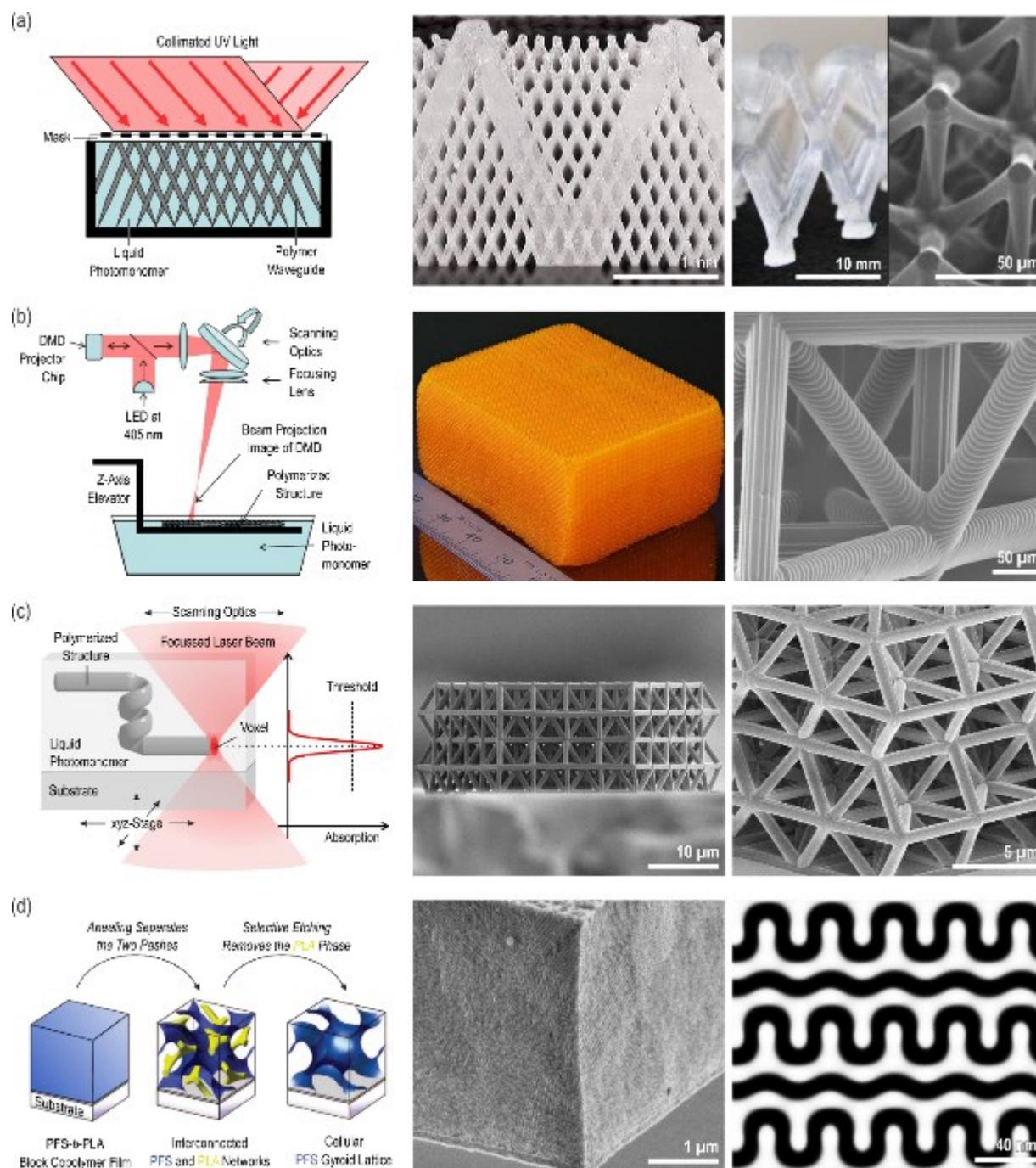
nanolattice fabrication tool.

Figure 9. Selected processes for fabricating micro- and nanolattices. (a) By UV-light exposure of a photomonomer through a two-dimensional mask, SPPW creates polymeric microlattices, tens of centimeters in size, within minutes; while topologies are limited to linear extensions of the mask, feature dimensions may be varied in a broad range, from >25 mm thick single unit cell structures to lattices with members ~10 µm in diameter, to hierarchical structures. (b) Large area PµSL creates centimeter-size arbitrary polymeric microstructures with minimal feature dimensions of 5-300 µm, in a layer-by-layer fashion by polymerizing the surface layer of a photomonomer bath through a digital mask. (c) DLW processes focus a laser

beam into a photomonomer, creating an ellipsoid shaped polymer feature (voxel) down to 100 nm in size, via multi-photon polymerization. Scanning the laser beam and moving the sample stage forms arbitrary micro- and nanostructures of typically <1 mm overall size. (d) Self-assembly i.e. of block copolymers like poly(4-fluorostyrene-block-D,L-lactide) (PFS-b-PLA), can create a number of topologies such as gyroid lattices, with feature sizes down to 10 nm and overall dimensions of up to centimeters. Adopted from [83,208] and reproduced with permission, [19] 2014 ,[15] 2011, The American Association for the Advancement of Science, [209] 2017, Nanoscribe GmbH, [107] 2015, Elsevier, [210] 2009, American Chemical Society.

3.5. Synthesis of Composite, Ceramic and Metal Structures

To date, there are no metal- or ceramic-based AM processes with sufficiently high resolution for the synthesis of nanolattices. The majority of fabrication techniques are polymer-based, and a number of post-processing techniques exist that are used to overcome this limitation.

Atomic layer deposition (ALD) is a highly conformal deposition process that allows for the coating of complex 3D geometries with angstrom-level thickness control.[211] ALD in its simplest form is a thermal process that works by depositing a monolayer of a precursor onto a surface then flowing a reactant over it, resulting in a single atomic layer of a given material. This cycle can be repeated until a specific material thickness is obtained. More complex forms of ALD can use multiple precursors and plasma ignition to facilitate less thermodynamically favorable chemical reactions. ALD is highly advantageous due to its lack of directional dependence and its ability to diffuse into small spaces, making it ideal for coating polymeric nanolattices to form core-shell composite structures[2,14] **(Figure 10a)**. Composite structures can be cut open, e.g. by focused ion beam milling, allowing for the removal of the polymer core by etching or thermal treatment.[13,198] The major limitation of ALD is its slow rate, which is normally on the order of nanometers per hour. ALD can be used to create a wide range of materials, including metals, ceramics, and semiconductors.[212]

Electroless plating of metals is a well-established method for coating a broad range of shapes and materials.[213] Preferred are metals with a reduction potential greater than that of water, so that they can be deposited in aqueous solutions. Ionic liquid based processes have been

developed for important metals with a low reduction potential such as aluminum. Electroless deposition is a favorable method for the coating of lattice materials with metals due to the conformal, non-line-of-sight deposition characteristics[15]. Electroless plating processes rely on an autocatalytic reaction to reduce the metal ions in solution; it therefore enables the uniform deposition into pores as long as mass transport is not limited. Hollow-beam metal lattices can be fabricated in a process analogous to that illustrated in Figure 10a.

Electroplating into negative templates enables the fabrication of solid-beam metallic lattices (Figure 10b).[9,89] This process involves first spinning a positive tone photoresist, i.e. a photoresist that is designed to be removed after exposure to UV light, onto a conductive substrate. Transparent conductive substrates can be made using thin films of indium tin oxide (ITO) or gold, which remain sufficiently transparent when sputtered at thicknesses of <50 nm. Using AM techniques, a structure can then be written into the photoresist, with the requirement that it must span from the top of the spun photoresist to the conductive substrate in order to ensure a conductive path. After the exposed resist has been developed, the pores can be infiltrated with an electroplateable material. Electroplating is a commonly utilized industrial process, and has been shown to offer a high degree of nanostructural material control.[214] In contrast to electroless plating, electroplating uses an applied voltage from an external source to deposit a material from solution. Deposition rates are proportional to the current density in the part, which also depends on the electric field applied by the anodes. The application of a constant voltage can result in a moderate directional dependence and deposition that is limited by line of sight. With advanced electroplating techniques such as voltage pulsing and conformal anodes, metal can readily be deposited into complex, three-dimensional nanoscale pores. Multiple metals can be electroplated in parallel, but complexity increases exponentially with every additional metal; electroplating is therefore not well suited for the creation of multicomponent alloys. Care must be taken to ensure that the electroplating solution does not

react with and erode the photoresist. After electroplating, the undeveloped photoresist can be removed using a developer, leaving behind a solid lattice.

Using *pyrolysis*, glassy carbon-based structures (Figure 10c) can be made from thermosetting polymers, such as UV-cured resins, that are thermally decomposed in vacuum or inert atmosphere at temperatures in the range of 1000-3000°C.[215] This process is accompanied by shrinkages of up to 90%.[216] Glassy carbon is an amorphous carbon allotrope that primarily consists of non-graphitic sp²-bonded carbon.[99,216] The fabrication of nanolattices using pyrolysis offers two unique benefits. (I) Polymer templates are directly transformed to robust ceramic structures, avoiding procedures like coating, milling and etching. Glassy carbon exhibits excellent chemical and thermal stability as well as biocompatibility and can achieve semiconductor-type electrical properties.[216] Its Young's modulus is about 10 times higher than that of cross-linked epoxy resins[217], and strengths in nanolattices on the order of 3 GPa have been observed. Its low density[99,215] of 1.3-1.5 g/cm³ is attributed to a fullerene-related closed-cell porosity[218]. Silicon-based pre-ceramic resins can be used to fabricate pre-ceramic polymer lattices via UV-curing, which then can be converted to ceramics such as silicon-oxycarbide[84]. (II) With appropriate designs, highly uniform shrinkage can be exploited to fabricate considerably smaller structures than what is achievable with the applied fabrication method alone. A five-fold reduction in size was demonstrated with direct-laser written octet lattices (Figure 10c).[1]

AM with *particle-loaded polymers* allows for the fabrication of macro- and microlattices from a variety of materials. The most common of these processes use inorganic particles like oxides embedded in a thermoset polymer that become sintered after the polymer is burned off[19]. Metal particles can also be used, and good results have been achieved with copper and silver.[219] Carbon fiber reinforced polymer composites[220] as well as foam based ceramic lattices[221] have also been processed. The major drawbacks of this method are that the final material is likely to

possess a high flaw population, and the reduced resolution and feature quality. Both of these makes particle-loaded AM techniques difficult to use for the fabrication of nanolattices. Lithographically defined microstructures of graphene oxide flakes with feature sizes on the order of 1 μm[222] as well as high-quality, transparent fused silica microstructures[223] have been shown, though.
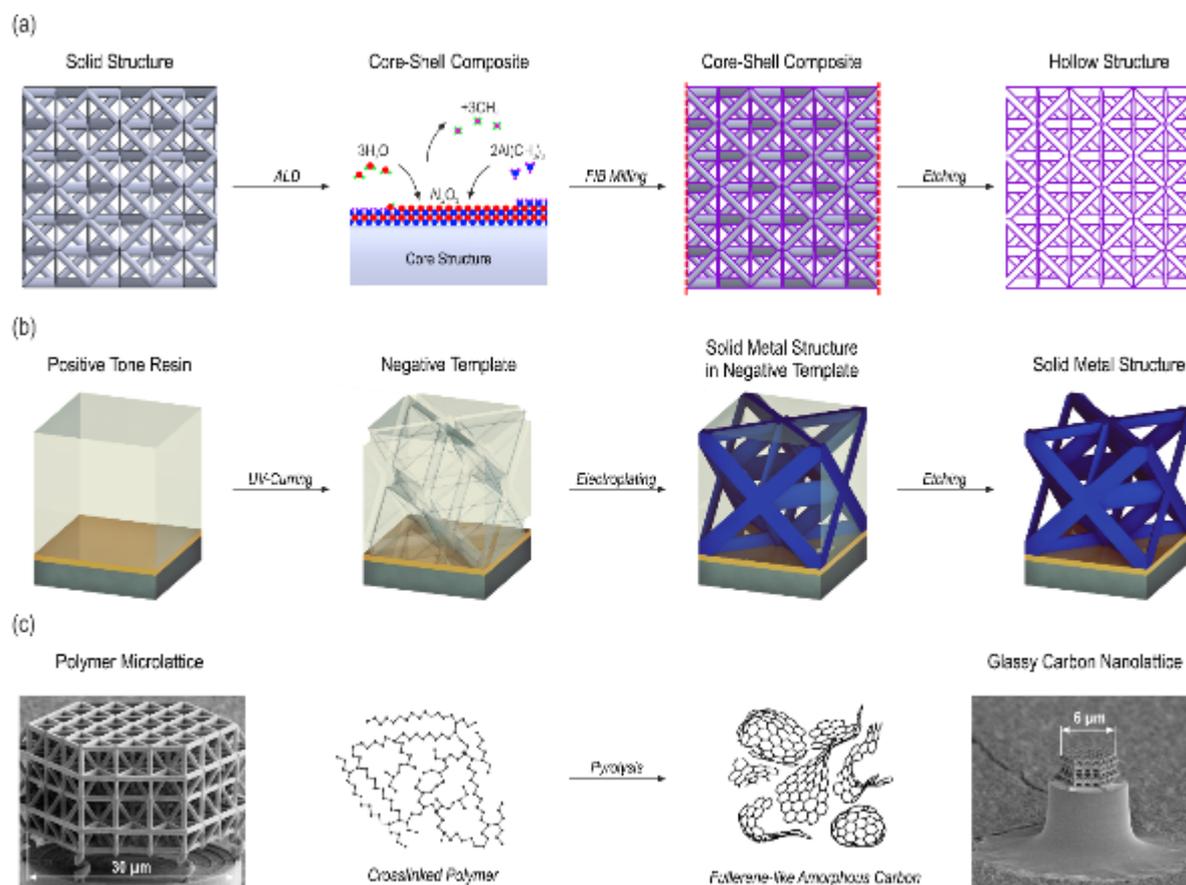

Figure 10. Post-processing routes for synthesizing ceramic, metallic and composite nanolattices based on polymer templates. (a) Hollow-beam ceramic lattices are fabricated by ALD, focused ion beam (FIB) milling and etching; analogously, metal lattices can be made via electroless plating. (b) Electroplating into a negative template creates solid-beam metal lattices. (c) Accompanied by conformal shrinkage of up to 90%, pyrolysis of polymer lattices yields carbon-based ceramic lattices. Adopted from [1] and reproduced with permission, [13] 2014, The American Association for the Advancement of Science, [89] 2015, Elsevier.

4. Hierarchical Architecture & Scale-Up

The exceptional properties of nanolattices can only truly have an impact as engineering materials if they are scaled-up to sizes that are relevant for technological applications. Scaling-up the dimensions of a structure while keeping its smallest feature sizes at the nanoscale is

inherently difficult, and current fabrication methods dictate a tradeoff between build volume, production rate and minimum feature size. The most straightforward workaround to overcome this problem is to combine large-scale, high-throughput processes with thin film deposition techniques to produce hollow structures, but any length scale gaps in the architecture will inevitably lead to shell buckling instabilities due to high ratios of diameter-to-wall-thickness[15].

Hierarchical architecture provides a means of expanding build volumes without sacrificing accuracy, resolution or structural integrity. The production rates of many AM processes scale proportionally to the relative density of the structure being manufactured. The effective relative density ($\bar{\rho}_{eff}$) of a hierarchical structure compounds with increasing hierarchical order, and for an architecture of order N is given approximately by

$$\bar{\rho}_{eff} = \prod_1^N \bar{\rho}_i, \tag{8}$$

where $\bar{\rho}_i$ is the relative density of the ith level of hierarchy. When the order of hierarchy is increased, the compounding relative densities decrease the effective relative density without increasing the slenderness of individual structural elements, thereby maintaining structural stability.

A scaled-up manufacturing of microlattices with nanoscale features from hundreds of micrometers to several centimeters has been demonstrated using large area PμSL.[83] **Figure 11** shows a breakdown of the feature sizes in these materials, the length scale of each order of structural hierarchy decreases by a factor of ~10 from one level to the next. The microlattice consists of a network of octet unit cells (Figure 11c) comprised of strut members that are ~200 μm in diameter, each of which consist of a network of self-similar smaller-scale unit cells (Figure 11h). The first-order unit cells are made from hollow tube nickel–based struts (Figure 11i) with diameters on the order of 10 μm and wall thicknesses ranging from 50 nm to 700 nm (Figure 11j). Similar orders of structural hierarchy has been shown in nanolattices made from

both core-shell polymer-alumina and hollow alumina with first-order strut diameters below 1 μm and shell thicknesses of 20 nm, and an overall structure size on the order of hundreds of micrometers.[82]
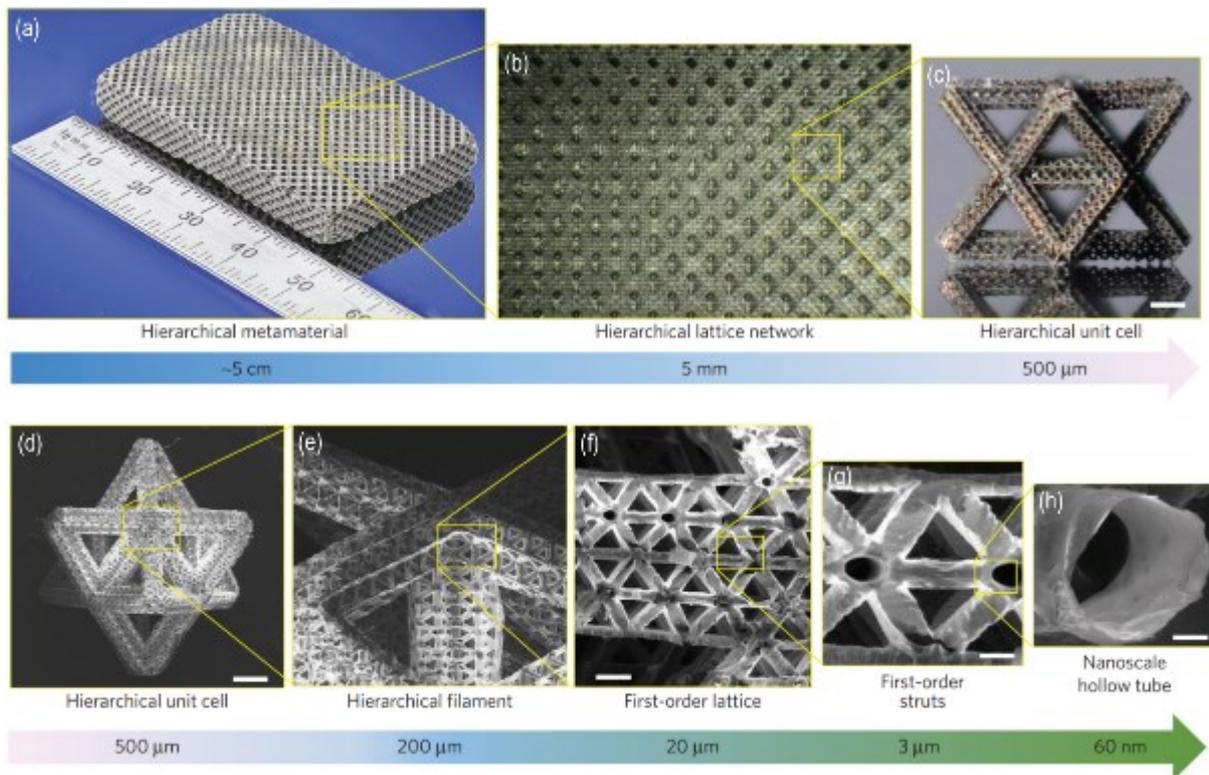

Figure 11. Centimeter-size hierarchical hollow-beam nickel microlattice material fabricated using large area projection micro-stereolithography. (a-c) Optical microscope images of bulk hierarchical lattice material with a network of hierarchical octet unit cells. (d)-(h) Scanning electron micrographs showing the breakdown of structural hierarchy down to hollow-beam walls tens of nanometers in thickness. The scale bar is 80 μm in (c) and 3 μm in (h). Adopted from [83].

Hierarchical architectures offer a range of unique mechanical properties that are widely taken advantage of in the natural world (Figure 3).[68,69] Diatom frustules, Euplectella glass sponges, and bone have exceptional resilience to mechanical loading. Soft tissues such as skin and structures like bird's nests are highly compliant and able to undergo large deformations without failure. A number of man-made structures have been created that have hierarchical architectures, the most common of which are construction cranes and building scaffolding, and the most notable example being the Eiffel tower[224]. One key advantage of both natural and engineered hierarchical structures is their increased resistance to buckling. Recalling the Euler buckling

criterion from Section 2.1.2, the buckling strength of a beam scales with its length as $1/l^2$, and the resulting strength of a buckling-dominated lattice scales with relative density as $\sigma \propto \bar{\rho}^2$. In a hierarchical structure, the relative densities at each order of hierarchy are multiplied according to Equation 8, meaning beam length and relative density are decoupled. The length of the beams can therefore be much shorter for a given $\bar{\rho}$ compared to a single-order structure, resulting in an increase in the buckling resistance.

There are four different types of hierarchical lattice architectures that can be created using stretching- and bending-dominated constituent lattices **(Figure 12)**.[49] Combinations of self-similar architectures at adjacent hierarchical levels result in fractal-like lattices that are either stretching-stretching or bending-bending. Combining dissimilar architectures at neighboring hierarchies results in hybrid lattices that are either stretching-bending or bending-stretching. In all four cases, the effective strength (σ_{eff}) of a hierarchical structure of order N can be approximated by the first order scaling law

$$\sigma_{eff} = C_{eff} \prod_1^N \bar{\rho}_i^{a_i} \sigma_s \tag{9}$$

where σ_s is the strength of the constituent solid material, C_{eff} is an effective geometric parameter, and a_i is the scaling exponent of each order. Similarly, the effective stiffness (E_{eff}) can be estimated by,

$$E_{eff} = F_{eff} \prod_1^N \bar{\rho}_i^{g_i} E_s \tag{10}$$

where E_s is the Young's modulus of the constituent solid material and F_{eff} is an effective geometric parameter.

First Order Architecture   Second Order Architecture

Stretching-Dominated   Bending-Stretching   Stretching-Stretching

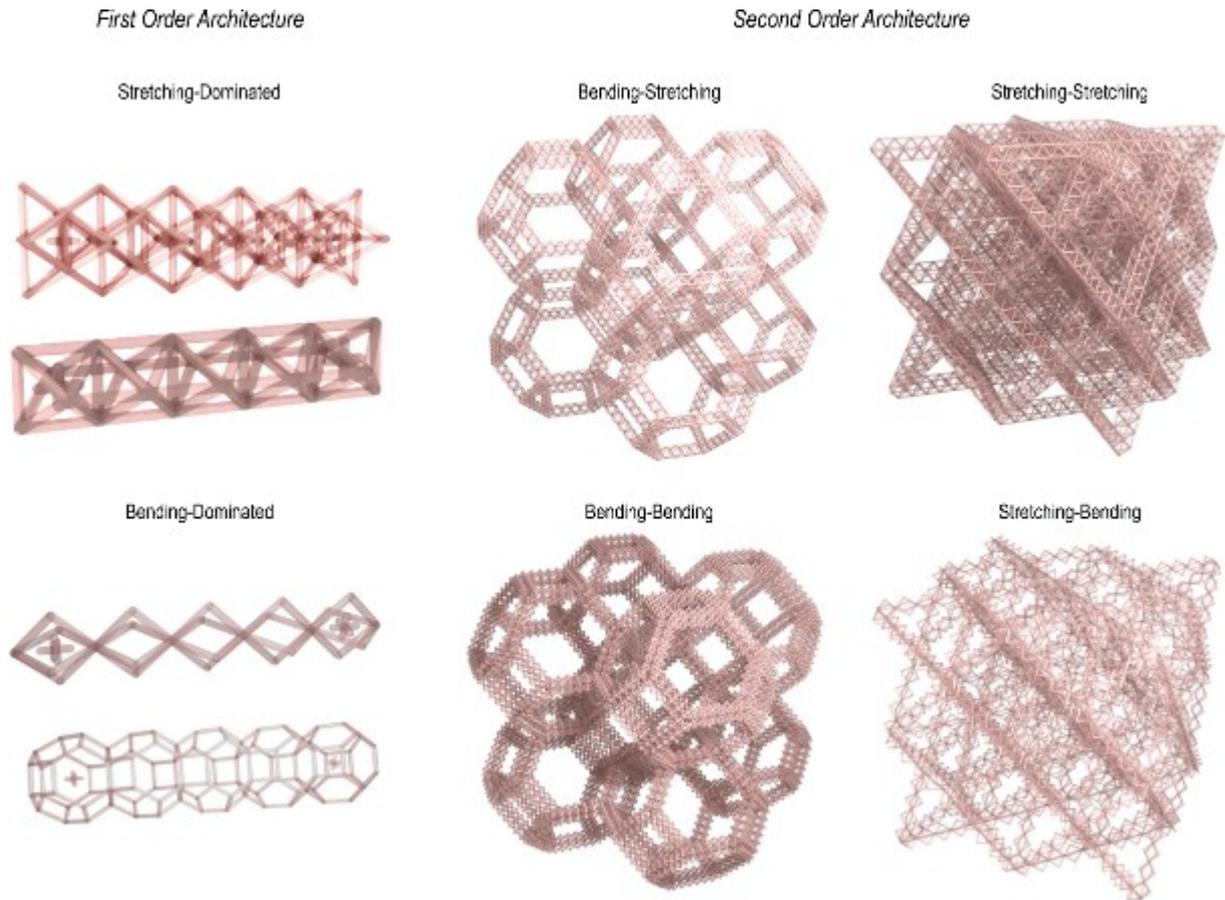Bending-Dominated   Bending-Bending   Stretching-Bending

Figure 12. Different types of hierarchical lattice architectures. Mechanical behavior can be tailored for high strength and stiffness (stretching-stretching), high compliance (bending-bending) or the intermediate cases of both (bending-stretching, stretching-bending). Adopted from [83].

Fractal-like stretching-dominated hierarchy can lead to superior strength at low density due to an increased buckling stability, potentially enabling access to ultra-low density material property spaces that are inaccessible to first order lattices. Tunable failure behavior and increased energy absorption has been demonstrated with lattices[82,83], honeycombs and sandwich panels[225–227], and corrugated truss[228] and space frame structures[229]. Fractal-like stretching-dominated micro-[83] and nanolattices[82] have exhibited near-linear scaling of strength and stiffness down to $\bar{\rho} \approx 0.01\%$ (Figure 4 and Figure 6), while corresponding first order lattices[13,19] have scaling exponents as high as 2.7 below $\bar{\rho} \approx 0.1\%$. The geometric parameters of the hierarchical orders have a multiplying effect due to the underutilization of non-axially oriented lattice elements; this can lead to a reduction in the effective properties. For

example, the effective geometric parameter of an octet lattice decreases from 1/3 to 1/9 as a structure goes from first- to second-order, which results in a decrease of σ_{eff} by a factor of three. This same mechanism has the effect of increasing the damage tolerance. After axially oriented lattice elements undergo failure, non-axially oriented elements are able to remain intact and distribute strain through bending or local elastic buckling, thereby accommodating large global deformation without failure.[82] Recoverabilities of up to 98% of the original structure height after compression to ≥50% have been reported.[82] Corresponding to Section 2.3, the introduction of hierarchy increases the tailorability of failure modes and post-failure behavior. Based on classical lattice theory, stiffness cannot be increased by the addition of hierarchy to the architecture, but it has been postulated that the introduction of hierarchy can reduce local bending effects in certain structures, leading to an increase in the effective stiffness.[82]

Fractal-like bending-dominated hierarchies can be used to create highly compliant structures. A second-order lattice with $g_1 = g_2 = 2$ has an effective scaling exponent between stiffness and relative density of four. This can potentially allow for large, super-elastic deformations even with brittle base materials. Combining bending-dominated architectures may not always result in an increased compliance. In contrast to stretching-dominated hierarchies, the geometric parameters of each bending-dominated hierarchical order adds up, leading to an increased effective stiffness.[226,230] This can be understood as a gain in flexural rigidity for a given relative density that occurs when replacing slender lattice elements with a bending-dominated network of smaller-scale, short and squat elements. A similar behavior applies for the effective strength.[226]

Combining stretching- and bending dominated architectures yields mixed behavior. A cuboid-octet microlattice optimized for tensile loading has been constructed by tessellating a first-order stretching-dominated topology with a second-order bending-dominated one.[83] The microlattice was comprised of brittle 60 nm nickel-based thin films but still demonstrated

reversible elastic stretching up to 20% strain; this was achieved while simultaneously attaining specific tensile strengths substantially higher than commercial foams and comparable to those of first order core-shell polymer-ceramic lattices[87] synthesized using DLW.[83] While the stiffness of these materials was governed by compliant hinges in the bending-dominated second order of hierarchy, their high strength has been attributed to mechanical size-effects in the hollow-beam walls of the first-order architecture. Ceramic honeycomb structures fabricated using direct foam writing with a bending-dominated first order topology and a stretching-dominated second order architecture were shown to possess highly tailorable stiffness.[221] The effective geometric parameter of bending-stretching architectures increases with the number of hierarchical orders in a similar manner to fractal-like bending architectures. The reverse is true for stretching-bending type architectures; as the elements of the stretching-dominated lattice are replaced by bending-dominated ones, they deform by bending instead of stretching, resulting in reduced stiffness compared to the first-order stretching-dominated architecture.

5. Conclusion & Outlook

The introduction of lattice architecture at the micro- and nanoscale has set new boundaries on the accessible regions of many material property spaces. Photonic and phononic metamaterials with periodicity comparable to the wavelength of optical or acoustic waves were the first drivers towards miniaturization. The high strengths of nanolattices for the first time strikingly demonstrated the ability to exploit size effects in mechanical metamaterials. Simultaneously nanolattice architecture can be designed to enable unique scale-independent properties such as tailorable stiffness, deformability, thermal expansion, as well as auxetic behavior and pentamode meta-fluidity. It is the confluence of nanomaterials and architecture that engenders the huge diversity of properties of nanolattices, although not all properties explicitly benefit from miniaturization.

The extensive work on nanolattices in the recent years has laid the foundation for this emerging field. Data is still very limited and key physical principles, including some of those described here, are the subject of some uncertainty. More in depth characterization and modeling are still required to draw a comprehensive picture. Due to experimental limitations, investigations into the mechanical behavior of nanolattices has mostly been limited to compression tests, and proper assessment of their tensile, shear, and fracture properties needs to be done. Besides strength, many more mechanical, or thermal and electrical properties exhibit size-dependent behavior. Incorporation of these effects in nanolattices would inevitably lead to major advances in the colonization of new material property space, and bears the potential for creating new materials with superior multifunctionality. Approaches for creating metamaterials may vary widely across disciplines, but it is remarkable how similar optimal architectures and scales often are. Moving forward, nanolattices should not be thought of as photonic, phononic, auxetic, or light-weight metamaterials, but instead as a single class of multifunctional materials. As nature shows, the introduction of hierarchy is crucial to achieve both multifunctionality and optimized individual properties like mechanical robustness. Initial efforts for the introduction of structural hierarchy into nanolattices have been promising, and eventual designs may be able to fully mimic the material hierarchy of biological materials, leading to a new generation of multifunctional nanolattice materials.

Size-effects in materials have been investigated for decades, and nanolattices provide a promising avenue for the preservation of superior size-affected properties in large-scale materials applications. A major future challenge will be to substantially push the current limits of scalability to create nanolattices with sizes that are relevant for technical applications. Some potential methods to increase production while maintaining nanoscale features are parallelization by diffractive beam splitting of laser techniques such as DLW, multi-step self-assembly, and hybrid fabrication methods that combine AM with extrusion or injection molding.

These fabrication methods have a number of technological challenges associated with their implementation, the most critical of which being that they avoid introducing macroscopic flaws that counteract the beneficial properties gained from using nanomaterials. Another challenge is extending the narrow bandwidth of materials available for manufacturing of nanolattices.

The first market for nanolattices may be small-scale, small-lot components for biomedical, electrochemical, microfluidic and aerospace applications, which require highly customizable and extreme combinations of properties. Should scalability become a reality, nanolattices will find application in a variety of lightweight structural components. Over the past few years, nanolattices have certainly caught the attention of scientists and engineers alike. The scientific and technological development over the next few decades will be critical for moving this exciting new class of materials from the lab bench to our everyday life.

References

[1]   J. Bauer, A. Schroer, R. Schwaiger, O. Kraft, *Nat. Mater.* **2016**, *15*, 438.
[2]   J. J. do Rosário, E. T. Lilleodden, M. Waleczek, R. Kubrin, A. Y. Petrov, P. N. Dyachenko, J. E. C. Sabisch, K. Nielsch, N. Huber, M. Eich, G. A. Schneider, *Adv. Eng. Mater.* **2015**, DOI 10.1002/adem.201500118.
[3]   J. J. do Rosário, J. B. Berger, E. T. Lilleodden, R. M. McMeeking, G. A. Schneider, *Extrem. Mech. Lett.* **2016**, *in press*, DOI 10.1016/j.eml.2016.07.006.
[4]   A. J. Jacobsen, W. B. Carter, S. Nutt, *Adv. Mater.* **2007**, *19*, 3892.
[5]   X. Zheng, J. Deotte, M. P. Alonso, G. R. Farquar, T. H. Weisgraber, S. Gemberling, H. Lee, N. Fang, C. M. Spadaccini, *Rev. Sci. Instrum.* **2012**, *83*, 125001.
[6]   S. Maruo, O. Nakamura, S. Kawata, *Opt. Lett.* **1997**, *22*, 132.
[7]   A. Selimis, V. Mironov, M. Farsari, *Microelectron. Eng.* **2014**, *132*, 83.
[8]   X. Li, H. Gao, *Nat. Mater.* **2016**, *15*, 373.
[9]   S. N. Khaderi, M. R. J. Scherer, C. E. Hall, U. Steiner, U. Ramamurty, N. A. Fleck, V. S. Deshpande, *Extrem. Mech. Lett.* **2016**, DOI 10.1016/j.eml.2016.08.006.
[10]   N. Kröger, *Curr. Opin. Chem. Biol.* **2007**, *11*, 662.
[11]   J. Parkinson, R. Gordon, *Trends Biotechnol.* **1999**, *17*, 190.
[12]   D. Losic, J. G. Mitchell, N. H. Voelcker, *Adv. Mater.* **2009**, *21*, 2947.
[13]   L. R. Meza, S. Das, J. R. Greer, *Science* **2014**, *345*, 1322.
[14]   J. Bauer, S. Hengsbach, I. Tesari, R. Schwaiger, O. Kraft, *Proc Natl Acad Sci USA* **2014**, *111*, 2453.
[15]   T. A. Schaedler, A. J. Jacobsen, A. Torrents, A. E. Sorensen, J. Lian, J. R. Greer, L. Valdevit, W. B. Carter, *Science* **2011**, *334*, 962.
[16]   L. Valdevit, S. W. Godfrey, T. a. Schaedler, A. J. Jacobsen, W. B. Carter, *J. Mater. Res.* **2013**, *28*, 2461.
[17]   A. Torrents, T. A. Schaedler, A. J. Jacobsen, W. B. Carter, L. Valdevit, *Acta Mater.* **2012**, *60*, 3511.
[18]   K. J. Maloney, C. S. Roper, A. J. Jacobsen, W. B. Carter, L. Valdevit, T. A. Schaedler, *APL Mater.* **2013**, *1*, DOI 10.1063/1.4818168.
[19]   X. Zheng, H. Lee, T. H. Weisgraber, M. Shusteff, J. DeOtte, E. B. Duoss, J. D. Kuntz, M. M. Biener, Q. Ge, J. A. Jackson, S. O. Kucheyev, N. X. Fang, C. M. Spadaccini, *Science* **2014**, *344*, 1373.
[20]   T. Bückmann, N. Stenger, M. Kadic, J. Kaschke, A. Frölich, T. Kennerknecht, C. Eberl, M. Thiel, M. Wegener, *Adv. Mater.* **2012**, *24*, 2710.
[21]   M. Kadic, T. Bückmann, N. Stenger, M. Thiel, M. Wegener, *Appl. Phys. Lett.* **2012**, *100*, DOI 10.1063/1.4709436.
[22]   T. Ergin, N. Stenger, P. Brenner, J. B. Pendry, M. Wegener, *Science* **2010**, *328*, 337.
[23]   J. Fischer, T. Ergin, M. Wegener, *Opt. Lett.* **2011**, *36*, 2059.
[24]   J. K. Gansel, M. Thiel, M. S. Rill, M. Decker, K. Bade, V. Saile, G. Von Freymann, S. Linden, M. Wegener, *Science* **2009**, *325*, 1513.
[25]   A. G. Bell, *Natl. Geogr. Mag.* **1903**, *14*, 219.
[26]   J. Baldwin, *BuckyWorks : Buckminster Fullers Ideas for Today*, Wiley, New York, **1996**.
[27]   E. Arzt, *Acta Mater.* **1998**, *46*, 5611.
[28]   G. AA, *Phil Trans R Soc L. A* **1921**, *221*, 163.
[29]   H. Gao, B. Ji, I. L. Jaeger, E. Arzt, P. Fratzl, *Proc Natl Acad Sci USA* **2003**, *100*, 5597.
[30]   O. Kraft, P. A. Gruber, R. Mönig, D. Weygand, *Annu. Rev. Mater. Res.* **2010**, *40*, 293.
[31]   J. R. Greer, J. T. M. De Hosson, *Prog. Mater. Sci.* **2011**, *56*, 654.
[32]   L. H. Liang, B. Li, *Phys. Rev. B - Condens. Matter Mater. Phys.* **2006**, *73*, 1.

[33] A. a Balandin, S. Ghosh, W. Bao, I. Calizo, D. Teweldebrhan, F. Miao, C. N. Lau, *Nano Lett.* **2008**, *8*, 902.

[34] D. Josell, S. H. Brongersma, Z. Tőkei, *Annu. Rev. Mater. Res.* **2009**, *39*, 231.

[35] M. S. Dresselhaus, G. Chen, M. Y. Tang, R. Yang, H. Lee, D. Wang, Z. Ren, J. P. Fleurial, P. Gogna, *Adv. Mater.* **2007**, *19*, 1043.

[36] N. Hansen, *Scr. Mater.* **2004**, *51*, 801.

[37] T. Zhu, J. Li, S. Ogata, S. Yip, *MRS Bull.* **2009**, *34*, 167.

[38] G. Stan, S. Krylyuk, A. V. Davydov, I. Levin, R. F. Cook, *Nano Lett.* **2012**, *12*, 2599.

[39] X. Han, K. Zheng, Y. Zhang, X. Zhang, Z. Zhang, Z. L. Wang, *Adv. Mater.* **2007**, *19*, 2112.

[40] D.-M. Tang, C.-L. Ren, M.-S. Wang, X. Wei, N. Kawamoto, C. Liu, Y. Bando, M. Mitome, N. Fukata, D. Golberg, **2012**.

[41] D. Z. Chen, D. Jang, K. M. Guan, Q. An, W. A. Goddard, J. R. Greer, *Nano Lett.* **2013**, *13*, 4462.

[42] D. Jang, J. R. Greer, *Nat. Mater.* **2010**, *9*, 215.

[43] M. P. Manoharan, H. Lee, R. Rajagopalan, H. C. Foley, M. a. Haque, *Nanoscale Res. Lett.* **2010**, *5*, 14.

[44] C. Lee, X. Wei, J. W. Kysar, J. Hone, *Science* **2008**, *321*, 385.

[45] B. I. Yakobson, P. Avouris, in *Carbon Nanotub. Synth. Struct. Prop. Appl.* (Eds.: M.S. Dresselhaus, G. Dresselhaus, P. Avouris), Springer, Berlin, **2001**, pp. 287–327.

[46] K. Kawamura, G. Jenkins, *J. Mater. Sci.* **1970**, *5*, 262.

[47] A. Mathur, J. Erlebacher, *Appl. Phys. Lett.* **2007**, *90*, 2005.

[48] C. Ensslen, C. Brandl, G. Richter, R. Schwaiger, O. Kraft, *Acta Mater.* **2016**, *108*, 317.

[49] N. A. Fleck, V. S. Deshpande, M. F. Ashby, *Proc. R. Soc. A Math. Phys. Eng. Sci.* **2010**, *466*, 2495.

[50] V. S. Deshpande, M. F. Ashby, N. A. Fleck, *Acta Mater.* **2001**, *49*, 1035.

[51] L. J. Gibson, M. F. Ashby, *Cellular Solids: Structure and Properties*, Cambridge Univ. Pr., Cambridge, UK, **2001**.

[52] V. S. Deshpande, N. A. Fleck, M. F. Ashby, *J. Mech. Phys. Solids* **2001**, *49*, 1747.

[53] L. Dong, V. S. Deshpande, H. N. G. Wadley, *Int. J. Solids Struct.* **2015**, *60*, 107.

[54] T. George, V. S. Deshpande, H. N. G. Wadley, *Compos. PART A* **2013**, *47*, 31.

[55] L. Salari-Sharif, T. A. Schaedler, L. Valdevit, *J. Mater. Res.* **2014**, *29*, 1755.

[56] C. A. Steeves, S. L. dos Santos e Lucato, M. He, E. Antinucci, J. W. Hutchinson, A. G. Evans, *J. Mech. Phys. Solids* **2007**, *55*, 1803.

[57] J. T. B. Overvelde, T. A. de Jong, Y. Shevchenko, S. A. Becerra, G. M. Whitesides, J. C. Weaver, C. Hoberman, K. Bertoldi, *Nat. Commun.* **2016**, *7*, 10929.

[58] X. Hou, V. V Silberschmidt, in *Mech. Adv. Mater. Anal. Prop. Perform.* (Eds.: V. V Silberschmidt, V.P. Matveenko), Springer International Publishing, Cham, **2015**, pp. 155–179.

[59] R. Schittny, T. Bückmann, M. Kadic, M. Wegener, *Appl. Phys. Lett.* **2013**, *103*, 1.

[60] J. Christensen, M. Kadic, M. Wegener, O. Kraft, *MRS Commun.* **2015**.

[61] A. A. Zadpoor, *Mater. Horiz.* **2016**, *3*, 371.

[62] M. Maldovan, E. L. Thomas, *Periodic Materials and Interference Lithography: For Photonics, Phononics and Mechanics*, Wiley, **2009**.

[63] C. M. Soukoulis, M. Wegener, *Nat. Photonics* **2011**, *5*, 523.

[64] G. von Freymann, A. Ledermann, M. Thiel, I. Staude, S. Essig, K. Busch, M. Wegener, *Adv. Funct. Mater.* **2010**, *20*, 1038.

[65] M. Maldovan, *Nature* **2013**, *503*, 209.

[66] M. I. Hussein, M. J. Leamy, M. Ruzzene, *Appl. Mech. Rev.* **2014**, *66*, 40802.

[67] T. Bückmann, R. Schittny, M. Thiel, M. Kadic, G. W. Milton, M. Wegener, *New J. Phys.* **2014**, *16*, 33032.

[68]   P. Fratzl, R. Weinkamer, *Prog. Mater. Sci.* **2007**, *52*, 1263.

[69]   M. A. Meyers, P. Chen, A. Y. Lin, Y. Seki, **2008**, *53*, 1.

[70]   F. E. Round, R. M. Crawford, D. G. Mann, *Diatoms: Biology and Morphology of the Genera*, Cambridge University Press, Cambridge, UK, **1990**.

[71]   C. E. Hamm, R. Merkel, O. Springer, P. Jurkojc, C. Maier, K. Prechtel, V. Smetacek, *Nature* **2003**, *421*, 841.

[72]   S. Weiner, H. D. Wagner, *Annu. Rev. Mater. Sci.* **1998**, *28*, 271.

[73]   J. Aizenberg, J. C. Weaver, M. S. Thanawala, V. C. Sundar, D. E. Morse, P. Fratzl, *Science (80-.).* **2005**, *309*, 275.

[74]   J. Wolff, *The Law of Bone Remodeling*, Springer, Berlin, **1986**.

[75]   J. Currey, *Bones: Structure and Mechanics*, Princeton Univ Press, Princeton, **2002**.

[76]   A. G. M. Michell, *Philos. Mag. Ser. 6* **1904**, *8*, 589.

[77]   C. Mattheck, *Design in Nature : Learning from Trees*, Springer, Berlin, **1998**.

[78]   E. D. Yilmaz, S. Bechtle, H. Özcoban, A. Schreyer, G. a. Schneider, *Scr. Mater.* **2013**, *68*, 404.

[79]   M. A. Meyers, A. Y.-M. Lin, P.-Y. Chen, J. Muyco, *J. Mech. Behav. Biomed. Mater.* **2008**, *1*, 76.

[80]   A. Jantschke, C. Fischer, R. Hensel, H.-G. Braun, E. Brunner, *Nanoscale* **2014**, *6*, 11637.

[81]   C. Mattheck, *Die Körpersprache Der Bauteile: Enzyklopädie Der Formfindung Nach Der Natur*, Karlsruhe Institute Of Technology, Karlsruhe, **2017**.

[82]   L. R. Meza, A. J. Zelhofer, N. Clarke, A. J. Mateos, D. M. Kochmann, J. R. Greer, *Proc. Natl. Acad. Sci. U. S. A.* **2015**, *112*, 11502.

[83]   X. Zheng, W. Smith, J. Jackson, B. Moran, H. Cui, D. Chen, J. Ye, N. Fang, N. Rodriguez, T. Weisgraber, C. M. Spadaccini, *Nat. Mater.* **2016**, DOI 10.1038/nmat4694.

[84]   Z. C. Eckel, C. Zhou, J. H. Martin, A. J. Jacobsen, W. B. Carter, T. A. Schaedler, *Science (80-.).* **2016**, *351*, 58.

[85]   A. J. Jacobsen, S. Mahoney, W. B. Carter, S. Nutt, *Carbon N. Y.* **2011**, *49*, 1025.

[86]   S. J. Shin, S. O. Kucheyev, M. a. Worsley, A. V. Hamza, *Carbon N. Y.* **2012**, *50*, 5340.

[87]   J. Bauer, A. Schroer, R. Schwaiger, O. Kraft, *Adv. Eng. Mater.* **2016**, *18*, 1537.

[88]   M. Mieszala, M. Hasegawa, G. Guillonneau, J. Bauer, R. Raghavan, C. Frantz, O. Kraft, S. Mischler, J. Michler, L. Philippe, *Small* **2017**, *13*, 1602514.

[89]   X. W. Gu, J. R. Greer, *Extrem. Mech. Lett.* **2015**, *2*, 7.

[90]   L. C. Montemayor, J. R. Greer, *J. Appl. Mech.* **2015**, *82*, 1.

[91]   I. C. Cheng, A. M. Hodge, *Scr. Mater.* **2013**, *69*, 295.

[92]   J. R. Hayes, A. M. Hodge, J. Biener, A. V Hamza, K. Sieradzki, *J. Mater. Res.* **2006**, *21*, 2611.

[93]   C. A. Volkert, E. T. Lilleodden, D. Kramer, J. Weissmüller, *Appl. Phys. Lett.* **2006**, *89*, 87.

[94]   A. M. Hodge, J. Biener, J. R. Hayes, P. M. Bythrow, C. A. Volkert, A. V. Hamza, *Acta Mater.* **2007**, *55*, 1343.

[95]   J. Biener, A. M. Hodge, A. V. Hamza, L. M. Hsiung, J. H. Satcher, *J. Appl. Phys.* **2005**, *97*, 1.

[96]   S. O. Kucheyev, M. Stadermann, S. J. Shin, J. H. Satcher, S. A. Gammon, S. A. Letts, T. Van Buuren, A. V. Hamza, *Adv. Mater.* **2012**, *24*, 776.

[97]   S. a Steiner, T. F. Baumann, J. Kong, J. H. Satcher, M. S. Dresselhaus, *Langmuir* **2007**, *23*, 5161.

[98]   E. Krämer, S. Förster, C. Göltner, M. Antonietti, *Langmuir* **1998**, *14*, 2027.

[99]   F. C. Cowlard, J. C. Lewis, *J. Mater. Sci.* **1967**, *2*, 507.

[100] M. Berdova, T. Ylitalo, I. Kassamakov, J. Heino, P. T. Törmä, L. Kilpi, H. Ronkainen,

J. Koskinen, E. Hæggström, S. Franssila, *Acta Mater.* **2014**, *66*, 370.

[101] J. Lian, D. Jang, L. Valdevit, T. A. Schaedler, A. J. Jacobsen, W. B. Carter, J. R. Greer, *Nano Lett.* **2011**, *11*, 4118.

[102] M. A. Meyers, K. K. Chawla, *Mechanical Behavior of Materials*, Cambridge University Press, Cambridge, **2009**.

[103] A. Asadpoure, L. Valdevit, *Int. J. Solids Struct.* **2015**, *60–61*, 1.

[104] V. S. Deshpande, N. a. Fleck, *Int. J. Solids Struct.* **2001**, *38*, 6275.

[105] J. Zhang, M. F. Ashby, *Int. J. Mech. Sci.* **1992**, *34*, 475.

[106] P. M. Suquet, *J. Mech. Phys. Solids* **1993**, *41*, 981.

[107] J. Bauer, A. Schroer, R. Schwaiger, I. Tesari, L. Valdevit, O. Kraft, *Extrem. Mech. Lett.* **2015**, *3*, 105.

[108] S. C. Han, J. W. Lee, K. Kang, *Adv. Mater.* **2015**, *27*, 5506.

[109] M. G. Lee, J. W. Lee, S. C. Han, K. Kang, *Acta Mater.* **2016**, *103*, 595.

[110] Hall, *Proc. Phys. Soc. B* **1951**, *64*, 747.

[111] N. J. Petch, *J. Iron Steel Inst.* **1953**, *174*, 25.

[112] X. W. Gu, Z. Wu, Y.-W. Zhang, D. J. Srolovitz, J. R. Greer, *Nano Lett.* **2013**, *13*, 5703.

[113] X. W. Gu, C. N. Loynachan, Z. Wu, Y. Zhang, D. J. Srolovitz, J. R. Greer, *Nano Lett.* **2012**, *12*, 6385.

[114] J. X. Zhao, R. C. Bradt, P. L. J. Walker, *Carbon N. Y.* **1985**, *23*, 15.

[115] A. Liu, in *ASM Handb. Vol. 19, Fatigue Fract.*, ASM International, **1996**, pp. 980–1000.

[116] M. D. Groner, F. H. Fabreguette, J. W. Elam, S. M. George, *Chem. Mater.* **2004**, *16*, 639.

[117] D. W. Richerson, *Modern Ceramic Engineering: Properties, Processing, and Use in Design*, CRC Press Taylor & Francis Group, Boca Raton, **2006**.

[118] R. Dou, B. Derby, *Scr. Mater.* **2009**, *61*, 524.

[119] H. S. Ma, J. H. Prévost, R. Jullien, G. W. Scherer, *J. Non. Cryst. Solids* **2001**, *285*, 216.

[120] H. G. Allen, P. S. Bulson, *Background To Buckling*, McGraw-Hill Book Company, **1980**.

[121] A. J. Jacobsen, W. B. Carter, S. Nutt, *Acta Mater.* **2007**, *55*, 6724.

[122] R. M. Jones, *Buckling of Bars, Plates, and Shells*, Bull Ridge Corporation, **2006**.

[123] B. Haghpanah, L. Salari-Sharif, P. Pourrajab, J. Hopkins, L. Valdevit, *Adv. Mater.* **2016**, *28*, 8065.

[124] D. Restrepo, N. D. Mankame, P. D. Zavattieri, *Extrem. Mech. Lett.* **2015**, *4*, 52.

[125] S. Shan, S. H. Kang, J. R. Raney, P. Wang, L. Fang, F. Candido, J. A. Lewis, K. Bertoldi, *Adv. Mater.* **2015**, *27*, 4296.

[126] T. Frenzel, C. Findeisen, M. Kadic, P. Gumbsch, M. Wegener, *Adv. Mater.* **2016**, 5865.

[127] M. F. Ashby, *Materials Selection in Mechanical Design Third Edition*, Butterworth-Heinemann, Oxford, **2005**.

[128] J. H. Lee, L. Wang, S. Kooi, M. C. Boyce, E. L. Thomas, *Nano Lett.* **2010**, *10*, 2592.

[129] J. H. Lee, L. F. Wang, M. C. Boyce, E. L. Thomas, *Nano Lett.* **2012**, *12*, 4392.

[130] J. H. Lee, J. P. Singer, E. L. Thomas, *Adv. Mater.* **2012**, *24*, 4782.

[131] L. Wang, M. C. Boyce, C. Y. Wen, E. L. Thomas, *Adv. Funct. Mater.* **2009**, *19*, 1343.

[132] N. A. Fleck, X. Qiu, *J. Mech. Phys. Solids* **2007**, *55*, 562.

[133] H. C. Tankasala, V. S. Deshpande, N. A. Fleck, *J. Appl. Mech.* **2015**, *82*, 91004.

[134] M. R. O'Masta, L. Dong, L. St-Pierre, H. N. G. Wadley, V. S. Deshpande, *J. Mech. Phys. Solids* **2017**, *98*, 271.

[135] L. C. Montemayor, W. H. Wong, Y.-W. Zhang, J. R. Greer, *Sci. Rep.* **2016**, *6*, 20570.

[136] D. Jang, R. Maaß, G. Wang, P. K. Liaw, J. R. Greer, *Scr. Mater.* **2013**, *68*, 773.

[137] G. N. Greaves, A. L. Greer, R. S. Lakes, T. Rouxel, *Nat Mater* **2011**, *10*, 823.

[138] K. K. Saxena, R. Das, E. P. Calius, *Adv. Eng. Mater.* **2016**, *18*, 1847.

[139] J. C. Álvarez Elipe, A. Díaz Lantada, *Smart Mater. Struct.* **2012**, *21*, 105004.

[140] S. Hengsbach, A. Díaz Lantada, *Smart Mater. Struct.* **2014**, *23*, 87001.

[141] G. W. Milton, A. V. Cherkaev, *J. Eng. Mater. Technol.* **1995**, *117*, 483.

[142] M. Kadic, T. Bückmann, R. Schittny, P. Gumbsch, M. Wegener, *Phys. Rev. Appl.* **2014**, *2*, 1.

[143] M. Kadic, T. Bückmann, R. Schittny, M. Wegener, *New J. Phys.* **2013**, *15*, DOI 10.1088/1367-2630/15/2/023029.

[144] T. Bückmann, M. Thiel, M. Kadic, R. Schittny, M. Wegener, *Nat. Commun.* **2014**, *5*, 4130.

[145] D. Y. Kang, W. Lee, D. Kim, J. H. Moon, *Langmuir* **2016**, *32*, 8436.

[146] J. Kaschke, M. Wegener, *Opt. Lett.* **2015**, *40*, 3986.

[147] M. Elmeranta, G. Vicidomini, M. Duocastella, A. Diaspro, G. De Miguel, *Opt. Mater. Express* **2016**, *3*, 444.

[148] J. Fischer, M. Wegener, *Opt. Mater. Express* **2011**, *1*, 614.

[149] Z. Liu, X. Zhang, Y. Mao, Y. Y. Zhu, Z. Yang, C. T. Chan, P. Sheng, *Science (80-.).* **2000**, *289*, 1734.

[150] S. Krödel, C. Daraio, *Phys. Rev. Appl.* **2016**, *6*, 64005.

[151] M. F. Ashby, A. Evans, N. a Fleck, L. J. Gibson, J. W. Hutchinson, H. N. G. Wadley, *Metal Foams: A Design Guide*, Butterworth-Heinemann, Oxford, **2000**.

[152] L. Valdevit, A. J. Jacobsen, J. R. Greer, W. B. Carter, *J. Am. Ceram. Soc.* **2011**, *1*, 1.

[153] C. A. Steeves, M. Y. He, S. D. Kasen, L. Valdevit, H. N. G. Wadley, A. G. Evans, *J. Appl. Mech.* **2009**, *76*, 31014.

[154] L. Valdevit, A. Pantano, H. A. Stone, A. G. Evans, *Int. J. Heat Mass Transf.* **2006**, *49*, 3819.

[155] N. G. Dou, A. J. Minnich, *Appl. Phys. Lett.* **2016**, *108*, DOI 10.1063/1.4939266.

[156] R. Lakes, *Appl. Phys. Lett.* **2007**, *90*, DOI 10.1063/1.2743951.

[157] O. Sigmund, S. Torquato, *J. Mech. Phys. Solids* **1997**, *45*, 1037.

[158] J. B. Hopkins, K. J. Lange, C. M. Spadaccini, *J. Mech. Des.* **2013**, *135*, 61004.

[159] R. M. Panas, J. B. Hopkins, *Proc. Annu. Meet. Am. Soc. Precis. Eng. 29th Annu. Meet.* **2014**, 2.

[160] Q. Wang, J. A. Jackson, Q. Ge, J. B. Hopkins, C. M. Spadaccini, N. X. Fang, *Phys. Rev. Lett.* **2016**, *117*, 1.

[161] M. C. Orilall, U. Wiesner, *Chem. Soc. Rev.* **2011**, *40*, 520.

[162] D. B. Burckel, C. M. Washburn, A. K. Raub, S. R. J. Brueck, D. R. Wheeler, S. M. Brozik, R. Polsky, *Small* **2009**, *5*, 2792.

[163] X. Xia, C. V. Di Leo, X. W. Gu, J. R. Greer, *ACS Energy Lett.* **2016**, *1*, 492.

[164] W. . b Wang, M. . Ozkan, C. S. . b b Ozkan, *J. Mater. Chem. A* **2016**, *4*, 3356.

[165] P. Danilevicius, *J. Biomed. Opt.* **2012**, *17*, 81405.

[166] F. Klein, B. Richter, T. Striebel, C. M. Franz, G. Von Freymann, M. Wegener, M. Bastmeyer, *Adv. Mater.* **2011**, *23*, 1341.

[167] C. Peters, M. Hoop, S. Pané, B. J. Nelson, C. Hierold, *Adv. Mater.* **2016**, *28*, 533.

[168] D. W. Yee, M. D. Schulz, R. H. Grubbs, J. R. Greer, *Adv. Mater.* **2017**, 1605293.

[169] H. N. G. Wadley, *Phil Trans R Soc A* **2005**, *364*, 31.

[170] I. Gibson, D. W. Rosen, B. Stucker, *Additive Manufacturing Technologies*, Springer US, New York, **2015**.

[171] S. Yin, A. J. Jacobsen, L. Wu, S. R. Nutt, *J. Mater. Sci.* **2013**, *48*, 6558.

[172] G. S. Xu, G. Yang, J. Gong, *Adv. Mater. Res.* **2012**, *424–425*, 52.

[173] B. Golaz, V. Michaud, Y. Leterrier, J. A. E. Mnson, *Polymer (Guildf).* **2012**, *53*, 2038.

[174] C. E. Corcione, A. Greco, A. Maffezzoli, *Polymer (Guildf).* **2005**, *46*, 8018.

[175] R. Bail, J. Y. Hong, B. D. Chin, *J. Ind. Eng. Chem.* **2016**, *38*, 141.

[176] J. Choi, R. B. Wicker, S. Cho, C. Ha, S. Lee, *Rapid Prototyp. J.* **2009**, *15*, 59.

[177] R. Bail, A. Patel, H. Yang, C. M. Rogers, F. R. A. J. Rose, J. I. Segal, S. M. Ratchev, *Procedia CIRP* **2013**, *5*, 222.

[178] Y. De Hazan, J. Heinecke, A. Weber, T. Graule, *J. Colloid Interface Sci.* **2009**, *337*, 66.

[179] J. W. Lee, I. H. Lee, D.-W. Cho, *Microelectron. Eng.* **2006**, *83*, 1253.

[180] A. Badev, Y. Abouliatim, T. Chartier, L. Lecamp, P. Lebaudy, C. Chaput, C. Delage, *J. Photochem. Photobiol. A Chem.* **2011**, *222*, 117.

[181] S. Kirihara, in *Eng. Ceram. Curr. Status Futur. Prospect.*, **2016**, pp. 117–122.

[182] S. Kirihara, *Weld. World* **2016**, *60*, 697.

[183] C. Kermer, M. Rasse, G. Lagogiannis, G. Undt, A. Wagner, W. Millesi, *J. Cranio-Maxillo-Facial Surg.* **1998**, *26*, 360.

[184] B. Farkas, I. Romano, L. Ceseracciu, A. Diaspro, F. Brandi, S. Beke, *Mater. Sci. Eng. C* **2015**, *55*, 14.

[185] A. Alibeigloo, *Compos. Part B Eng.* **2016**, *98*, 225.

[186] P. Mueller, M. Thiel, M. Wegener, *Opt. Lett.* **2014**, *39*, 6847.

[187] J. S. Oakdale, J. Ye, W. L. Smith, J. Biener, *Opt. Express* **2016**, *24*, 186.

[188] L. J. Jiang, Y. S. Zhou, W. Xiong, Y. Gao, X. Huang, L. Jiang, T. Baldacchini, J.-F. Silvain, Y. F. Lu, *Opt. Lett.* **2014**, *39*, 3034.

[189] L. Valdevit, J. Bauer, in *Three-Dimensional Microfabr. Using Two-Phot. Polym.* (Ed.: T. Baldacchini), Elsevier, Amsterdam, **2015**, pp. 345–373.

[190] H. Namatsu, K. Yamazaki, K. Kurihara, *J. Vac. Sci. Technol. B Microelectron. Nanom. Struct.* **2000**, *18*, 780.

[191] G. M. Whitesides, B. Grzybowski, *Science (80-.).* **2002**, *295*, 2418.

[192] W. Bai, C. A. Ross, *MRS Bull.* **2016**, *41*, 100.

[193] P. F. W. Simon, R. Ulrich, H. W. Spiess, U. Wiesner, **2001**, 3464.

[194] C. A. Ross, K. K. Berggren, J. Y. Cheng, Y. S. Jung, J. B. Chang, *Adv. Mater.* **2014**, *26*, 4386.

[195] M. R. J. Scherer, L. Li, P. M. S. Cunha, O. A. Scherman, U. Steiner, *Adv. Mater.* **2012**, *24*, 1217.

[196] V. Z. H. Chan, J. Hoffman, V. Y. Lee, H. Iatrou, A. Avgeropoulos, N. Hadjichristidis, R. D. Miller, E. L. Thomas, *Science (80-.).* **1999**, *286*, 1716.

[197] J. H. Pikul, S. Ozerinc, R. Zhang, P. V. Braun, W. P. King, *Proc. IEEE Int. Conf. Micro Electro Mech. Syst.* **2016**, *2016–Febru*, 451.

[198] J. H. Pikul, Z. Dai, X. Yu, H. Zhang, T. Kim, P. V Braun, W. P. King, *J. Micromechanics Microengineering* **2014**, *24*, 105006.

[199] X. Chen, L. Wang, Y. Wen, Y. Zhang, J. Wang, Y. Song, L. Jiang, D. Zhu, *J. Mater. Chem.* **2008**, *18*, 2262.

[200] A. H. Lu, F. Schüth, *Adv. Mater.* **2006**, *18*, 1793.

[201] M. H. Kim, S. H. Im, O. O. Park, *Adv. Mater.* **2005**, *17*, 2501.

[202] K. P. Velikov, C. G. Christova, R. P. A. Dullens, A. van Blaaderen, *Science (80-.).* **2002**, *296*, 106.

[203] R. P. Wesolowski, A. P. Terzyk, *Phys. Chem. Chem. Phys.* **2016**, *18*, 17018.

[204] V. V. Mitrofanov, M. M. Slepchenkov, G. Zhang, O. E. Glukhova, *Carbon N. Y.* **2017**, *115*, 803.

[205] Z. Qin, G. S. Jung, M. J. Kang, M. J. Buehler, *Sci. Adv.* **2017**, *3*, e1601536.

[206] V. Varshney, S. S. Patnaik, A. K. Roy, G. Froudakis, B. L. Farmer, *ACS Nano* **2010**, *4*, 1153.

[207] R. K. Paul, M. Ghazinejad, M. Penchev, J. Lin, M. Ozkan, C. S. Ozkan, *Small* **2010**, *6*, 2309.

[208] A. J. Jacobsen, J. A. Kolodziejska, K. D. Fink, C. Zhou, C. S. Roper, W. B. Carter, in *Solid Free. Fabr. Symp. Proc.*, **2010**.

[209] Nanoscribe GmbH, *Photonic Professional (GT) User Maual*, **2017**.

[210] E. J. W. Crossland, M. Kamperman, M. Nedelcu, C. Ducati, U. Wiesner, D.-M. Smilgies, G. E. S. Toombes, M. A. Hillmyer, S. Ludwigs, U. Steiner, H. J. Snaith, *Nano Lett.* **2009**, *9*, 2807.

[211] S. M. George, *Chem. Rev.* **2010**, *110*, 111.

[212] A. M. Schwartzberg, D. Olynick, *Adv. Mater.* **2015**, *27*, 5778.

[213] G. O. Mallory, J. B. Hajdu, *Electroless Plating: Fundamentals and Applications*, William Andrew Publishing, New York, **1990**.

[214] L. P. Bicelli, B. Bozzini, C. Mele, L. D'Urzo, *Int. J. Electrochem. Sci.* **2008**, *3*, 356.

[215] O. Schueller, S. Brittain, *Chem. Mater.* **1997**, *4756*, 1399.

[216] Y. Lim, J. Heo, M. Madou, H. Shin, *Nanoscale Res. Lett.* **2013**, *8*, 1.

[217] A. Mcaleavey, G. Coles, R. L. Edwards, W. N. Sharpe, *MRS Proc.* **1998**, *546*, DOI doi:10.1557/PROC-546-213.

[218] P. J. F. Harris, *Philos. Mag.* **2004**, *84*, 3159.

[219] B. Y. Ahn, S. B. Walker, S. C. Slimmer, A. Russo, A. Gupta, S. Kranz, E. B. Duoss, T. F. Malkowski, J. a Lewis, *J. Vis. Exp.* **2011**, 1.

[220] B. G. Compton, J. A. Lewis, *Adv. Mater.* **2014**, *26*, 5930.

[221] J. T. Muth, P. G. Dixon, L. Woish, L. J. Gibson, J. A. Lewis, *Proc Natl Acad Sci USA* **2017**, *114*, 1832.

[222] B. Senyuk, N. Behabtu, A. Martinez, T. Lee, D. E. Tsentalovich, G. Ceriotti, J. M. Tour, M. Pasquali, I. I. Smalyukh, *Nat. Commun.* **2015**, *6*, 7157.

[223] F. Kotz, K. Arnold, W. Bauer, D. Schild, N. Keller, K. Sachsenheimer, T. M. Nargang, C. Richter, D. Helmer, B. E. Rapp, *Nature* **2017**, *544*, 337.

[224] M. Sundaram, G. Ananthasuresh, *Resonance* **2009**, *14*, 849.

[225] A. Ajdari, B. Haghpanah Jahromi, J. Papadopoulos, H. Nayeb-hashemi, A. Vaziri, *Int. J. Solids Struct.* **2012**, *49*, 1413.

[226] B. Haghpanah, R. Oftadeh, J. Papadopoulos, A. Vaziri, *Proc. R. Soc. A Math. Phys. Eng. Sci.* **2013**, *469*, 1.

[227] R. Lakes, *Nature* **1993**, *361*, 511.

[228] G. W. Kooistra, V. S. Deshpande, H. N. G. Wadley, *J. Appl. Mech.* **2007**, *74*, 259.

[229] D. Rayneau-Kirkhope, Y. Mao, R. Farr, *Phys. Rev. Lett.* **2012**, *204301*, 1.

[230] R. Oftadeh, B. Haghpanah, D. Vella, A. Boudaoud, A. Vaziri, *Phys. Rev. Lett.* **2014**, *104301*, 1.

Jens Bauer received a M.S. (Dipl.-Ing.) degree in mechanical engineering from the Karlsruhe Institute of Technology (KIT), Germany, and completed his PhD at KIT's Institute for Applied Materials under Prof. Oliver Kraft. He received a research fellowship from the Deutsche Forschungsgemeinschaft (DFG) to study the multifunctional properties of nanoarchitected materials, and is currently a research associate at the University of California, Irvine working with Prof. Lorenzo Valdevit.

Lucas Meza completed his M.S. and PhD at the California Institute of Technology (Caltech) under the guidance of Prof. Julia R. Greer for his research on the Mechanical Properties of 3D Nanoarchitected Materials. He is currently a research associate at the University of Cambridge studying the micromechanics of 3D woven composite materials with Prof. Vikram Deshpande.

Tobias A. Schaedler is a Senior Research Scientist at HRL Laboratories, LLC, the former Hughes Research Labs in Malibu, CA, where he is developing new materials and manufacturing processes for aerospace and automotive applications. His current focus is on architected microlattices and truss core structures as well as on expanding the portfolio of ceramics and metal alloys suitable for additive manufacturing. He conducted undergraduate studies at the University of Bayreuth in Germany and then received a PhD in Materials Science from the University of California at Santa Barbara in 2006.